The Response of a Steep-Sided, Narrow Canyon to Time-Variable Wind Forcing

BARBARA M. HICKEY

School of Oceanography, University of Washington, Seattle, Washington

(Manuscript received 9 August 1994, in final form 2 October 1996)

ABSTRACT

The response of a relatively narrow (~7 km wide) and deep (~450 m deep) steep-sided (up to 45° bottom slope) submarine canyon to strong wind forcing is explored using data from an 18-element moored array as well as CTD surveys in the vicinity of Astoria submarine canyon. The data are used to describe spatial patterns and phase relationships between lateral velocity, vertical velocity, temperature, relative and stretching vorticity, alongshelf wind, and the flow incident on the canyon.

Upwelling within the canyon is simultaneous and spatially uniform to zero order, and vertical velocity is highly correlated and in phase with alongshelf wind. Vertical velocity within the canyon is not related to flow incident on the canyon except during strong upwelling. Above the canyon, temperature, rather than vertical velocity (time rate of change of temperature), is in phase with wind. Estimated vertical velocities within the canyon were as great as 50 m d^{-1} (upward) during upwelling and 90 m d^{-1} (downward) during wind relaxation following upwelling events.

At depths ~100 m above the canyon the flow field is undisturbed by the canyon topography. At depths ~40–100 m above the canyon, a cyclonic circulation pattern occurs, but only during conditions of weak incident flow (i.e., Rossby number <0.25). At depths ~80 m below the canyon rim, cyclonic vorticity is in phase with alongshelf wind and with vertical velocity: minimum cyclonic vorticity (or weak anticyclonic vorticity) is coincident with maximum upwelling and southward (upwelling favorable) wind, and maximum cyclonic vorticity is coincident with maximum downwelling and minimum southward wind (or weak northward wind).

1. Introduction

The field study described in this paper addresses the problem of time-variable stratified flow over steep topography, in this case, over a submarine canyon. Topographically trapped circulation patterns have been observed over topographic highs such as ridges and seamounts (Eide 1979; Gould et al. 1981) and also over topographic depressions (Cannon 1972; Freeland and Denman 1982; Church et al. 1984). Due to the complexity of the problem, only the steady aspects of such features have previously been described. Although some time series measurements have been made within submarine canyons (e.g., Shepard et al. 1979; Hunkins 1988; Noble and Butman 1989) most have been made along canyon axes, precluding detailed study of the three-dimensional circulation. The importance of submarine canyons to coastal processes and results from previous studies are described in detail in Hickey (1995).

The dataset presented herein is unique because the data were obtained at spatial and temporal scales sufficiently small to resolve the time-dependent circulation over the steep slopes of the topography. Moreover, the time period sampled with the moored array includes two striking upwelling events and at least one downwelling event to strongly force the circulation and the density field. Fortuitously, an extensive CTD survey took place during one of the strong upwelling events, and the increased spatial resolution provided by the CTD data on that one occasion was an important factor in determining the time-dependent canyon response to the variable forcing. The goals of this paper are 1) to describe the response of the canyon to strong wind forcing in as much detail as the dataset allows, 2) to provide an observation-based framework for the next generation of numerical models on time-variable flow over steep topography, and 3) to demonstrate the limitations of the present dataset in order to allow improved experimental design for future studies over steep coastal topography.

The initial analysis of this dataset utilized a purely statistical approach (Hickey 1987). Results demonstrated the existence of a topographically trapped cyclonic circulation pattern over the canyon for both the mean and the fluctuating flow. The statistics suggested that the maximum development of the cyclonic circulation lagged the maximum southward velocity in the incident flow by 1 or more days. The mechanism for the vortex development and, in particular, the lag between the

Corresponding author address: Dr. Barbara M. Hickey, School of Oceanography, University of Washington, Box 357940, Seattle, WA 98195.
E-mail: bhickey@u.washington.edu

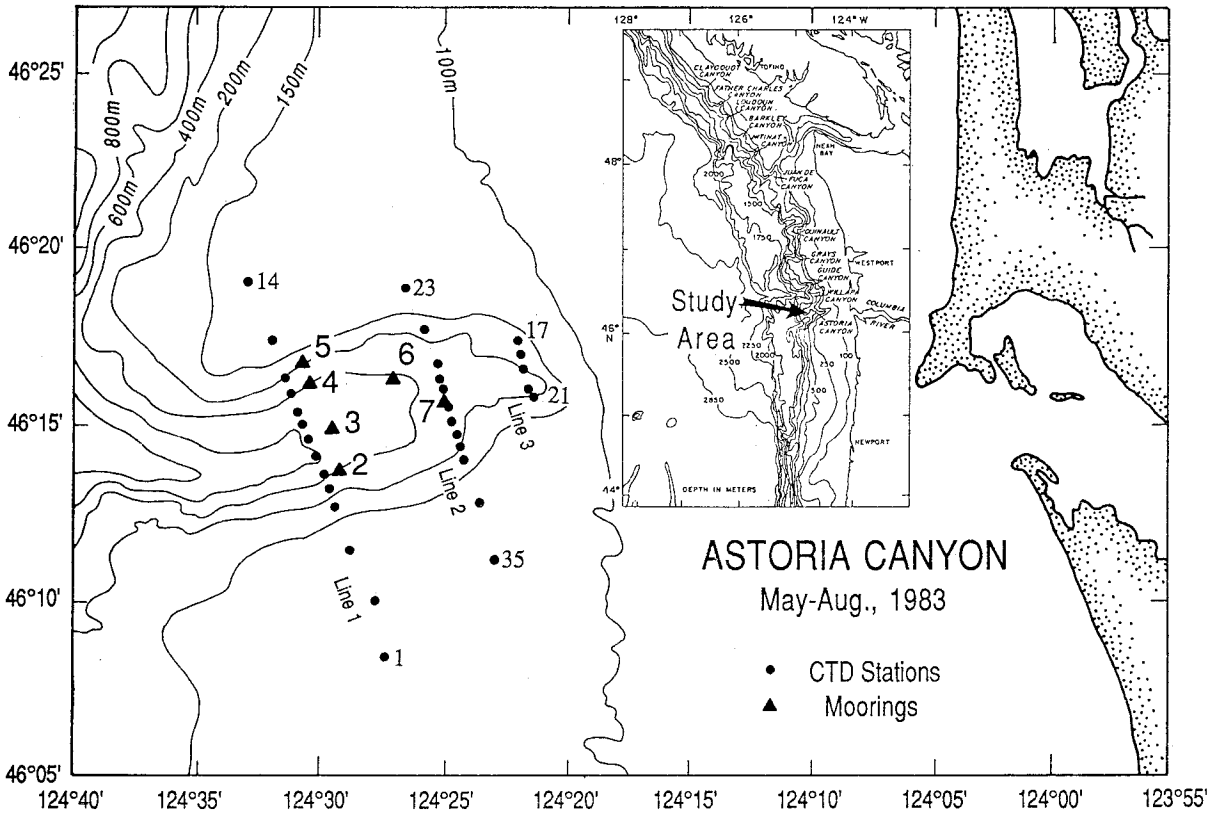

FIG. 1. Setting of Astoria submarine canyon with respect to the coastal topography. Locations of current meter arrays for the May–August 1983 deployment and of CTD stations for the May 1983 survey are shown on the figure. Mooring designations and station numbers for the beginning and end of each CTD section are also given on the map.

strength of the incident flow and that of the vortex could not be explained by the purely statistical approach. This paper extends the statistical results with a careful examination of time-dependent vertical and lateral displacement of flow layers over and within the canyon and with an analysis of the canyon vorticity field.

The paper is organized as follows. Bathymetric and environmental settings are described in section 2. Data and pertinent analyses are given in section 3. Section 4 presents the time-dependent currents measured in the vicinity of the canyon and the regional currents and winds. The horizontal velocity field is described in more detail in section 5, and the hydrographic variability as well as estimates of vertical velocity are presented in section 6. These descriptions are integrated in section 7 into an analysis of the spatial and temporal vorticity fields, including both stretching and relative vorticity. The observational results are compared with results from available models in section 8 and results are summarized in section 9. For the reader's assistance, a schematic illustrating data-derived characteristic timescales and spatial patterns of alongshelf wind, vertical and lateral velocity, temperature, and vorticity fields during spinup and spindown from an upwelling event is included in the summary.

2. Setting

The canyon studied is situated off the U.S. West Coast just offshore of the Columbia River (Fig. 1). The river plume itself is confined to the upper ~20 m of the water column and thus, as we will see, is unlikely to have significant interaction with either canyon processes or its topography. To compare with other studies of flow over steep topography, it is useful to describe the setting and the topographic anomaly in terms of several nondimensional numbers. For Astoria Canyon, the axial bottom depth (H) is 600 m, the depth of the canyon from its rim to the bottom (h_m) is 450 m, and the half-width (L) is 3.5 km. Thus, the fractional height (h_m/H) is 0.75 and the aspect ratio (H/L) is 0.2. The variable and strong forcing over Astoria Canyon induces significant variability in the Rossby number (Ro $= U/fL$), where U is the time-variable incident velocity and f is the Coriolis parameter, as well as the stratification parameter ($S = NH/fL$), the vertical stratification scale (Tr $= fL/N$), and the internal Rossby radius of deformation ($R_d = NH/f$), each of which depends on the stratification through the buoyancy frequency [$N^2 = (g/\rho)(\partial\rho/\partial z)$], where g is the acceleration due to gravity, ρ is density, and z is positive downward. For the observed range of

average and maximum incident flows over the period considered (10–30 cm s^{-1}), Ro ranges from about 0.05 to 0.6; N varies from about 5×10^{-3} to 10×10^{-3} s^{-1}. Thus, the stratification parameter (S) ranges from about 8 to 16, the vertical stratification scale (Tr) ranges from about 80 to 40 m, and the internal Rossby radius (R_d) ranges from about 30 to 60 km, for weak and strong stratification, respectively.

Astoria Canyon is ''very'' narrow; that is, the canyon width is much less than the local internal Rossby radius of deformation. Astoria Canyon is also ''very'' deep, that is, the depth of the canyon below its rim is roughly three times the depth of the incident flow (~450 m vs 150 m). The canyon shoals slightly toward the head. The walls of Astoria Canyon are steep, approaching 45° in some locations. The steepness combined with the excellent fishing makes the area an extremely difficult place to make in situ current measurements. The canyon is relatively symmetrical in shape and is aligned such that the canyon axis is roughly perpendicular to the direction of the local isobaths. Since the alongshelf currents are quasigeostrophic, the regional flow follows the northwest to southeast direction of the local isobaths (Hickey 1989). Hence the regional flow direction intersects the canyon axis at roughly right angles.

The seasonal variation of currents over the Washington shelf and slope is described in detail in Hickey (1989). In general, the mean flow is northward in late fall and winter and southward in spring and summer. During summer, this pattern is complicated by the existence of a northward undercurrent over the outer shelf and slope. Unfortunately, Astoria Canyon intersects the shelf at the approximate depth of the undercurrent velocity maximum, which further complicates the analysis of the canyon circulation. Event-scale (several day) current fluctuations with large alongshelf scales (>500 km) are superimposed on the seasonal means. These fluctuations are generally forced by local wind (especially during winter) or are a result of remote wind forcing (especially during spring and summer). In general, northward wind events result in northward flow and downwelling over the shelf and upper slope, and southward wind events result in southward flow and upwelling. Typical currents near the shelf break are ~20 cm s^{-1}, but peak speeds up to 50 cm s^{-1} in spring and 100 cm s^{-1} in winter are not uncommon (Hickey 1989; Hickey et al. 1997, manuscript submitted to *J. Geophys. Res.*). A strong El Niño event (1982–83) was occurring during the period of the measurements. The effects of this El Niño in the Pacific Northwest, in particular, a dramatic (1°–2°C) warming of the water column and increased persistence of northward flow, are described in a series of papers in the book by Wooster and Fluarty (1985).

3. The data

The study described in this paper was partially motivated by an earlier study that was designed to determine to what extent the canyon perturbs the regional shelf circulation at mid water column depths. Velocity vectors from this experiment demonstrated that canyon topography had little effect on the circulation on the adjacent shelf as well as over the canyon (Fig. 2). On the other hand, cross-canyon hydrographic sections showed large density perturbations (Fig. 2.48 in Hickey 1989). Sigma-t contours were consistent with upwelling from depths of 200–300 m within the canyon up over the rim of the canyon. At depths near the rim, isopycnals on the north side of the canyon were consistent with vertical stretching of density layers, such as might occur when a water column is forced to flow into a region of increased depth.

Motivated by these results, a second study was designed to sample both the velocity and mass fields within and near the canyon itself. To ensure a coherent array, moorings were placed at closely spaced (~2–5 km) intervals both along and across the canyon (Fig. 1). Moorings are identified by a number followed by the depth of a specific sensor; for example, A7, 94 refers to the current meter at 94 m on mooring 7, whose location is shown in Fig. 1. The array was deployed from May to August 1983. Two moorings over the shelf along the seaward transect were lost due to fishing activities, and a number of the other moorings were damaged by fishermen and prematurely returned. One mooring was recovered using the deep submersible *Alvin.* Time series range in duration from two weeks to three months.

Moorings were of a subsurface, taut-wire configuration, with the uppermost float at a depth of at least 65 m from the sea surface. Aliasing by surface waves is minimal in the relatively quiescent spring–summer season. Aanderaa current meters were used on all moorings, and data were obtained at 20-minute intervals. These data were filtered to obtain hourly data and further filtered to remove tidal and inertial oscillations. This low-passed dataset was subsampled at 6-h intervals to produce the subtidal dataset used in the analysis.

Hydrographic data including light transmission were obtained at the beginning and end of the deployment period of the fixed instrument array (21 May, 22 May, and 18 August). The May survey consisted of three transects across the canyon, two of which correspond roughly to the mooring transects (Fig. 1).

The CTD data were obtained with a Neil Brown CTD, calibrated with in situ salinity samples. Data were edited to 1-m intervals. Light transmission (LT) from the 0.25-cm pathlength transmissometer was converted to beam attenuation (A) using the formula

$$A = -\ln\mathrm{LT}/0.25$$

(Hickey et al. 1986).

Vertical fluctuations of isopycnals due to the semidiurnal tide can be particularly energetic in submarine canyons due to focusing by the topography (Hotchkiss and Wunsch 1982; Baines 1983). The canyon stations in the CTD sections were obtained over a period of

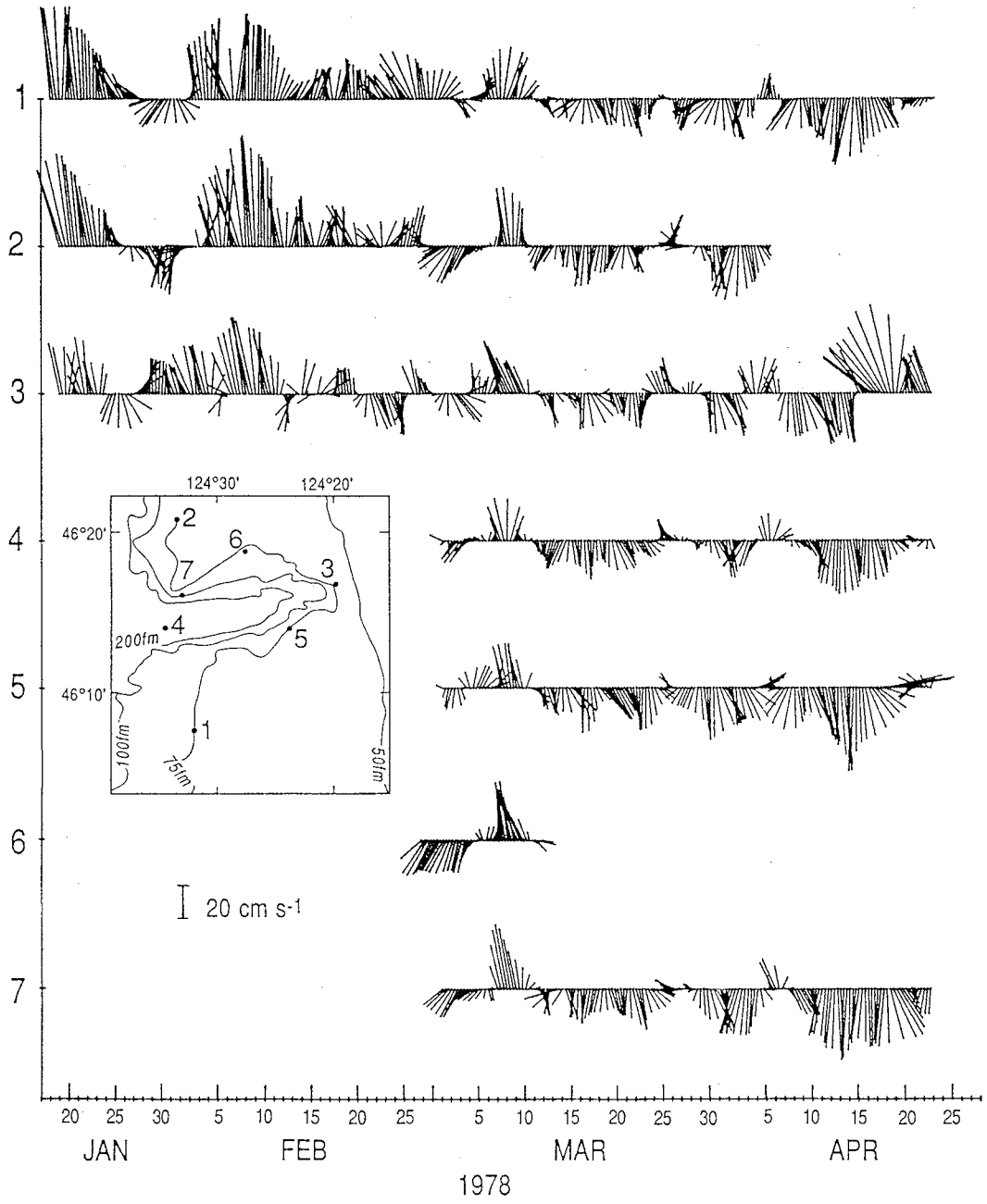

FIG. 2. Subtidal velocity vectors ~60 m from the sea surface on the axis of Astoria Canyon and on the adjacent shelf during January–April 1978. Vectors are given in a north–south, east–west reference frame.

about 5 h and so might be subject to tidal aliasing. To determine specific tidal effects at selected depths during the CTD surveys, we compared CTD data treated as a time series with hourly data from the moored array (not shown). Results suggest that, although the cross-canyon structure on 21 May does not appear to be tidal, the 10–20 m depression of isopleths observed near the canyon rim on 22 May could be tidal in origin. A direct estimate of the effects of tides was recently obtained with a 15-h time series during an upwelling event in June 1995 at midcanyon along the line 1 transect of the 1983 survey. Vertical excursions of isopleths due to the semidiurnal internal tide at that time were about 25 m, 30 m, and 50 m at depths of 125 m (above the canyon rim), 200 m (just below the rim), and 400 m (deep in the canyon), respectively (not shown). Discussion of the CTD data is limited to features that exceed these excursions.

Local wind data were not available for the duration of the experiment. Bakun wind (derived from atmo-

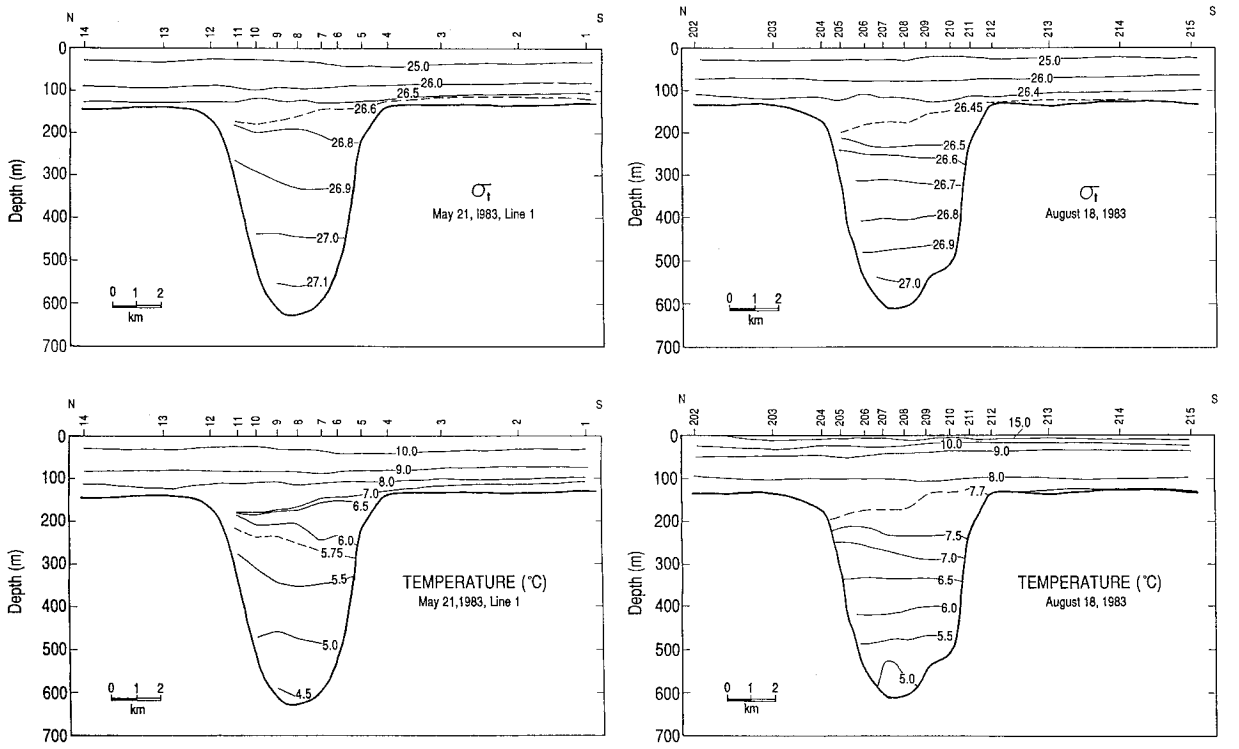

FIG. 3. Temperature and sigma-t contoured on north–south sections across Astoria Canyon on 21 May 1983 and on 18 August 1983. The location of the section on 21 May relative to the canyon topography is shown in Fig. 1. The 18 August section is in approximately the same location as the 21 May section. Station numbers are given along the top of each section.

spheric pressure data gridded at 3° intervals) is used to describe the regional wind field (Bakun 1975). Because the dominant wind scales in this region are known to exceed 500 km (Halliwell and Allen 1987), Bakun wind should provide a reasonable indicator of primary wind events during the study. To avoid emphasizing possible noise by squaring wind amplitudes, wind stress was not computed; wind data are used as a proxy for wind stress data.

Because no data are available on the shelf near Astoria Canyon, data from a mid-Oregon midshelf region 300 km south of Astoria Canyon (mooring Q3 in the SuperCODE experiment; 43°9.5′N, 124°34.6′W) are used to provide an indicator of the regional currents. Fluctuations in currents in the Oregon–Washington region have been shown to be strongly correlated over distances up to 500 km (Huyer et al. 1975).

To enable use of the moored temperature data, the analysis was performed on temperature rather than density data. This substitution is justified because temperature and density are linearly related in this region and because no temperature inversions were observed in the CTD data. A comparison of temperature and density sections for the 21 May and 18 August surveys illustrates that all major features in the density field are replicated in the temperature field (Fig. 3).

4. Time-dependent forcing

Velocity vectors show that, in general, the closer the measurement depth to the sea surface, the more the flow passes directly across the canyon; the closer the measurement depth to the rim of the canyon, the more the flow turns cyclonically around the canyon topography (Fig. 4). For example, at both north and south sites on the canyon rim, flow 94 and 70 m below the surface (~60 and 80 m above the canyon rim) is directed across the local isobaths (Fig. 4, left side). However, flow 134 m from the surface on the north rim (~20 m below the rim) is directed west-southwest on the north rim and flow at 110 m on the south rim (~40 m above the rim) is directed southeast. The flow at locations several kilometers east of the principal canyon transect demonstrates that the cyclonic circulation pattern is also observed below the canyon rim (Fig. 4, right side). At such depths the mean flow appears to be roughly parallel to the local isobaths rather than across them.

Large amplitude fluctuations are superimposed on the mean flow field (Fig. 4). In particular, several strong southward flow events are observed in the first month of the records. Comparison of the north–south component of flow at one site with temperature below the canyon rim at that site demonstrates that these southward flow events are associated with the appearance of

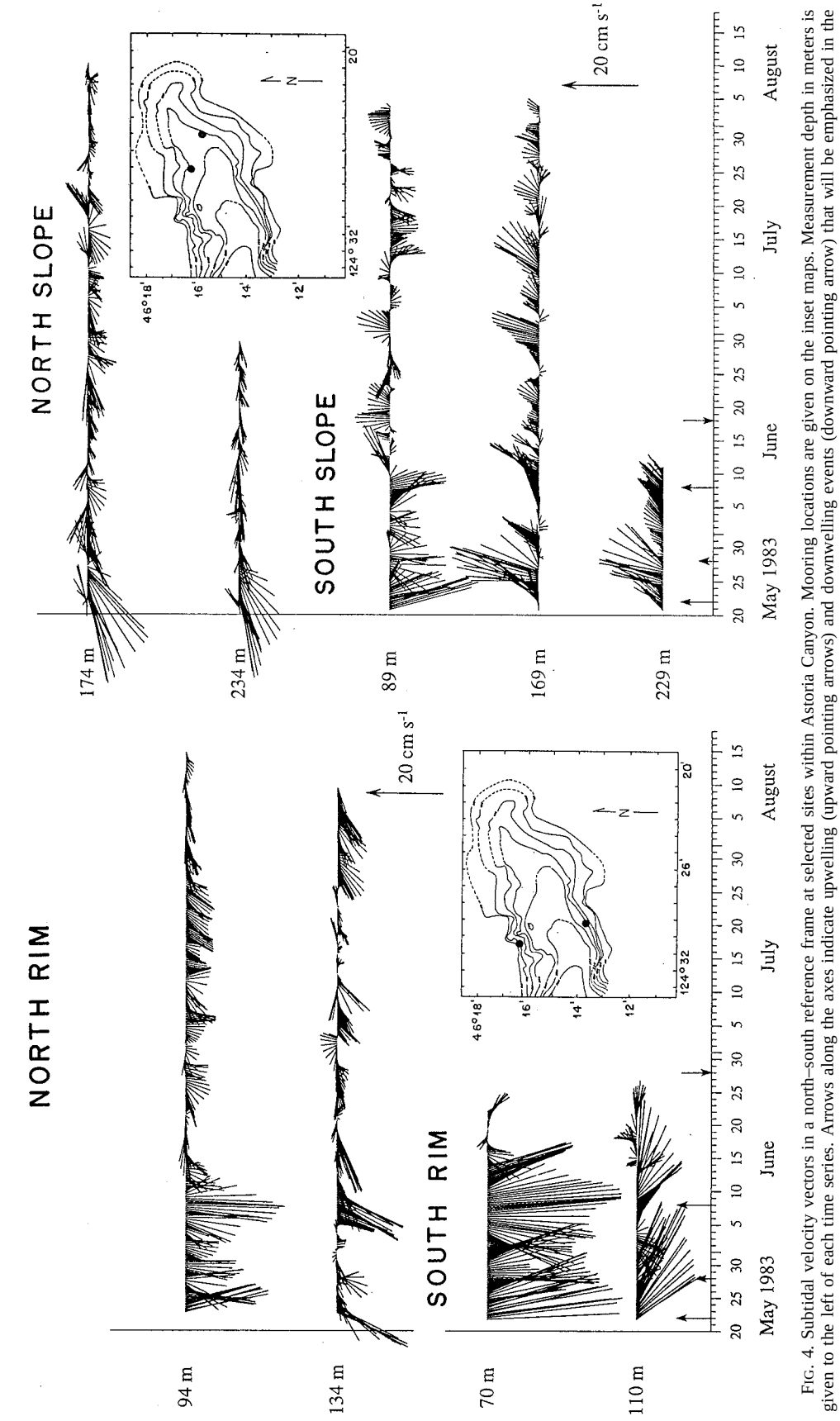

FIG. 4. Subtidal velocity vectors in a north–south reference frame at selected sites within Astoria Canyon. Mooring locations are given on the inset maps. Measurement depth in meters is given to the left of each time series. Arrows along the axes indicate upwelling (upward pointing arrows) and downwelling events (downward pointing arrow) that will be emphasized in the text. To orient the reader these arrows are reproduced in the majority of the figures that follow.

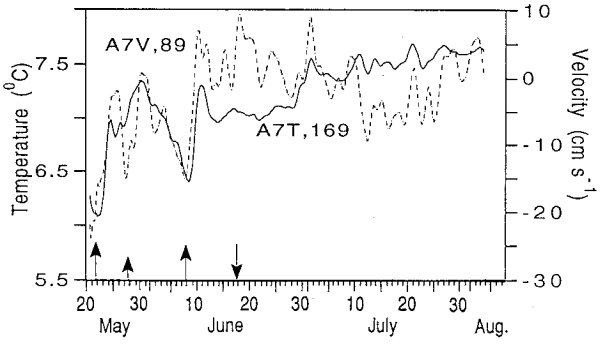

FIG. 5. Subtidal time series of north–south velocity (positive northward) at mooring A7 at a depth of 89 m from the sea surface (A7V, 89) and temperature at a depth of 169 m at the same mooring location (A7T, 169). The flow at A7 at 89 m is thought to be representative of regional flow incident upon the canyon. The temperature at A7 at 169 m is representative of temperature below the canyon rim.

colder water within the canyon (Fig. 5). The velocity fluctuations are significantly correlated to alongshelf wind ($r = 0.62$) with a lag of 1.25 d for maximum correlation (Fig. 6, upper left). The lag between wind and current is somewhat larger than that expected in this region for alongshelf and quasigeostrophic flow generated by local alongshelf wind stress (Hickey 1989). Comparison between the flow over the canyon with that at a midshelf site off Oregon (Fig. 6, lower right) shows that the Astoria currents, although significantly correlated to the Oregon currents, lag those off Oregon by about a day (Fig. 6, upper right). As much as half of the Astoria–Oregon lag could be due to differences in frictional effects at the two sites: the Astoria site is on the outer shelf (bottom depth ~150 m), whereas the Oregon site is at midshelf (bottom depth ~100 m) (see e.g., Brink et al. 1987). The lag is also consistent with the existence of significant low-mode coastal-trapped wave activity during the measurement period. Previous studies have demonstrated that low-mode coastal-trapped waves forced by the large-scale wind field, are commonly observed in the Pacific Northwest

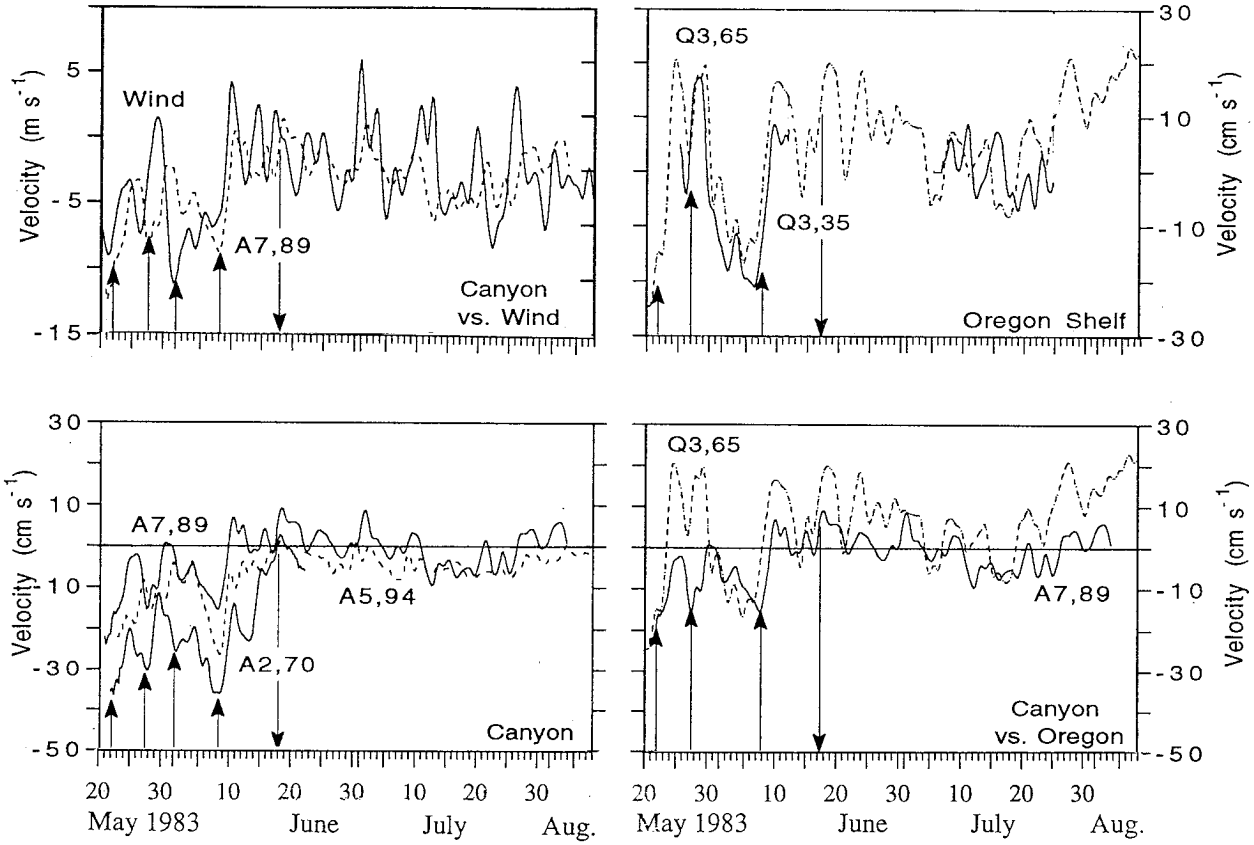

FIG. 6. Upper right: Time series of the north–south component of subtidal velocity (positive northward) at 35 m (Q3, 35) and 65 m (Q3, 65) at a midshelf site off Oregon. Lower right: Time series of the north–south component of subtidal velocity ~60 m above the rim of Astoria Canyon (A7, 89) and at a midshelf site off Oregon (Q3, 65). Upper left: Time series of the north–south component of subtidal velocity incident on Astoria Canyon (A7, 89) and the north–south component of Bakun wind computed at a latitude of 46°N. Lower left: Time series of the north–south component of subtidal velocity (positive northward) at three sites within the canyon at depths >50 m above the canyon rim. Locations are shown in Fig. 1.

in spring and summer (Battisti and Hickey 1984). Such waves would typically give rise to time lags of about 0.6 d between currents at the two sites.

In summary, the several strong alongshelf current events observed in the first month of the canyon records are regional in nature, and they are forced by large-scale alongshelf wind. A significant portion of the current variance appears to be remotely forced. The currents and winds are associated with regional upwelling (for southward wind) or regional downwelling (for northward wind). Three upwelling events (two strong and one weak) and one downwelling event during this period have been selected for discussion and are identified with vertical arrows at the same exact time in all figures for the reader's reference. The arrows marking the upwelling events are placed to coincide with minimum temperatures in the canyon at a depth of about 400 m. The downwelling event had no visible signature in temperature time series at mid water column and deeper depths. The arrow corresponding to this event was therefore placed to coincide with the onset of upper-layer flow northward across the isobaths on the south side of the canyon (i.e., at A2, 70).

It is difficult to determine which of the available time series provides the best estimate for flow incident on the canyon. For example, the alongshelf flow above the canyon rim at the several canyon sites differs significantly between the sites with respect to both the mean flow and the timing of events (compare A2, 70 and A7, 89 in Fig. 6, lower left). Also, the mean flow in all of the canyon records is more southward than at the Oregon midshelf site (Fig. 6, lower right). This difference might be due to the fact that the canyon data are from the outer shelf, whereas the Oregon data are from midshelf. Because the Oregon and Washington data have significant differences (for whatever reason), it is unlikely that the Oregon data are representative of flow incident on the canyon. In the subsequent analysis we have elected to use the current record at A7 at a depth of 89 m from the surface (most similar to the Oregon midshelf record with respect to mean flow characteristics) to represent flow incident on the canyon.

Although flow in the near-surface layers over the shelf is generally southward at this time of year (Hickey 1989), northward flow occurs a significant fraction of the time in the 1983 records, particularly at the Oregon site. This is likely due to the fact that a major El Niño event was underway at the time of these measurements. El Niño is typically associated with warmer water and more persistent northward flow along the coast. The effects of the 1982–83 El Niño on currents, temperature, and sea level over the Pacific Northwest shelf are described in detail by Huyer and Smith (1985). The persistent northward flow in the latter half of the canyon record might also be due to the presence of the northward undercurrent typically observed over the shelf and slope during summer and early fall. However, the lack of significant vertical shear at the Oregon shelf site suggests that no strong undercurrent existed, at least over the shelf, during the measurement period (Fig. 6, upper right). Hydrographic sections from the Oregon coast in 1983 suggest that an undercurrent was not present over the shelf or over the slope on 11–12 May but that it was likely present by 12 July at depths exceeding 250 m (Huyer and Smith 1985). Data from the Washington shelf ~100 km north of Astoria Canyon on 19–20 May, one day prior to the start of our measurements, also show no evidence of an undercurrent over the shelf or slope at that time (not shown). Based on these results, we will assume that during the period emphasized in the analysis (20 May–20 June) no undercurrent was present in the upper 250 m of the water column.

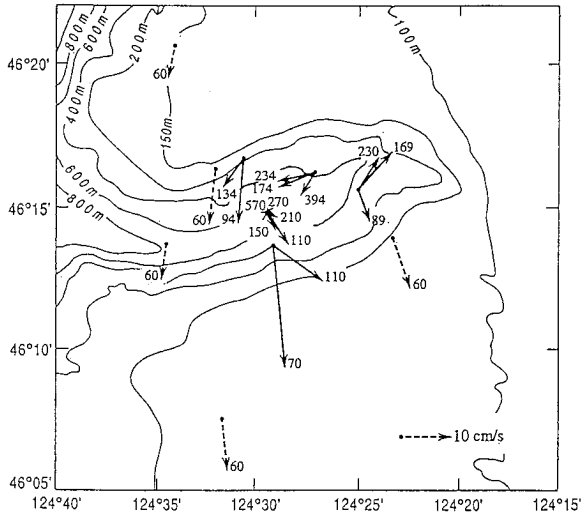

FIG. 7. Mean vector velocities within and over Astoria Canyon for 23 May–11 June 1983 (solid arrows) and 1 March–22 April 1978 (dashed arrows). The mean for A3, 150 was computed from data for the period 23 May–3 June. Measurement depth in meters is indicated near the tip of each vector.

5. The horizontal velocity field

a. Mean flow

Mean velocity vectors confirm the existence of cyclonic circulation over and within the canyon in spring 1983, with speeds of about 10 cm s^{-1} (Fig. 7). Means from a period of southward flow in late winter 1978 are included to provide more spatial information in the far field and the upper water column. The data illustrate that mean flow in the upper water column (60–70 m from the sea surface or ~90 m above the canyon rim) crosses directly over the canyon. However, within ~50 m of the canyon rim (depths >100 m from the sea surface), flow turns across the canyon isobaths, forming a cyclonic vortex over the canyon and its walls. Below the canyon rim (depths >150 m from the sea surface), the mean flow over the canyon walls is roughly aligned in the direction of the local isobaths and mean flow over

the canyon axis is across-canyon, roughly perpendicular to the isobaths. The height above the canyon to which the flow is disturbed by the canyon topography is roughly consistent with scales suggested for quasigeostrophic flow; that is, the mean vertical stratification scale is about 60 m over the measurement period.

Mean flow above the canyon on its north side is directed *offshore* of the canyon— slightly at 94 m; more strongly at deeper depths. Time series data at this site show that the flow at that location is much less frequently northward in comparison to other canyon sites at similar depths as well as to the Oregon data (Fig. 6). This suggests that even during periods when northward, rather than southward, flow is incident on the canyon, the ''V'' shape of the shelf edge on the north side of the canyon forces the flow southwestward along the north side of the canyon into the ''V'' and hence across the local isobaths.

b. Fluctuating flow

Sequential maps of the horizontal velocity field during three upwelling events and one downwelling event demonstrate clearly an organized temporal evolution of the velocity field during these events (Fig. 8). During each upwelling event, at maximum upwelling (i.e., when temperature is coldest, as indicated with vertical arrows in Fig. 5), the water column above the canyon[1] flows across the canyon, whereas up-canyon flow is observed at most locations below the rim of the canyon (21 May, 28 May, 8 June). As upwelling begins to weaken, the direction of flow below the canyon rim changes from up-canyon to down-canyon at locations on the north side of the canyon and to stronger up-canyon flow on the south side of the canyon (23 May, 30 May, 9 June). Maximum cyclonic circulation generally occurs one or two days after maximum upwelling (24 May, 30 May, 10 June), when alongshelf incident velocity has begun to weaken.

Time series of flow at selected sites just above and just below the canyon rim demonstrate the tendency for up-canyon flow on one side of the canyon to be roughly in phase with down-canyon flow on the other side and vice versa over the complete record (Fig. 9a). Note that at or just prior to the occurrence of minimum temperature within the canyon (indicated with upward pointing vertical arrows), down-canyon flow below the canyon rim on the north side of the canyon is briefly interrupted (diminished, if not reversed) by up-canyon flow. Maximum opposing flow on the two sides of the canyon occurs several days following the occurrence of coldest water in the canyon and the magnitude of the down-canyon flow that follows the occurrence of minimum temperature is roughly proportional to the temperature deficit caused by the upwelling event (see temperatures in Fig. 5).

The downwelling event selected for discussion is the only downwelling event during which the flow direction on the north side of the canyon actually reverses direction. During this event, flow on the south side of the canyon at 70 and 110 m from the surface is directed across the canyon isobaths as it was during the strong upwelling events, only in the opposite direction (northward instead of southward) (Fig. 8). The tendency for flow on the north side of the canyon to cross isobaths during the downwelling event is weak in comparison to the tendency for cross-isobath flow on the south side of the canyon during upwelling events. For example, at the height of the downwelling event on 18 June, the flow at 94 m on the north side of the canyon is almost due west, in comparison to the southeastward flow at 110 m on the south side during the 8 June upwelling event. This result supports the idea that the particular shape of this canyon funnels the flow on its north side toward the southwest. The circulation pattern during the downwelling event is primarily cyclonic both above and below the canyon rim. The onset of cyclonic circulation below the rim does not lag the incident velocity by several days as it does during upwelling.

Up-canyon and down-canyon flow below the canyon rim is significantly correlated with alongshelf wind (Fig. 9b, upper panel). Up-canyon flow is associated with maximum southward wind and down-canyon flow with minimum southward wind (denoted a ''relaxation'' from southward wind) or weak northward wind. Up-canyon flow lags southward wind by about 0.5 d; down-canyon flow is almost in phase with wind. Correlation with the flow incident on the canyon is also statistically significant; up-canyon flow is almost in phase with maximum incident flow but maximum down-canyon flow *precedes* minimum incident flow by 1–3 d (Fig. 9b, lower panel).

The decoupling of the flow incident on and above the canyon from the circulation within the canyon is demonstrated statistically by empirical orthogonal eigenfunction analysis of the east–west and north–south components of the velocity field: the first EOF describes primarily flow within the canyon or near the rim; the second describes primarily flow across the canyon isobaths above the canyon and up the canyon axis (for southward incident flow) below the canyon rim (Fig. 10). The amplitude time series of the second EOF is strongly related to time series of the alongshelf velocity of the incident flow field (A7, 89) (not shown). Thus, the axial up-canyon flow below the rim in this EOF is the signature of the up-canyon flow that occurs at the beginning of each regional upwelling event. The second EOF (representing the regional flow field) is significantly correlated at the 95% level with the first EOF

[1] To assist the reader ''up-canyon'' and ''down-canyon'' are used to describe flow within the canyon that is eastward (positive) or westward (negative), respectively. No vertical motion is implied by this terminology. Currents in this paper are always described in an east–west, north–south reference frame.

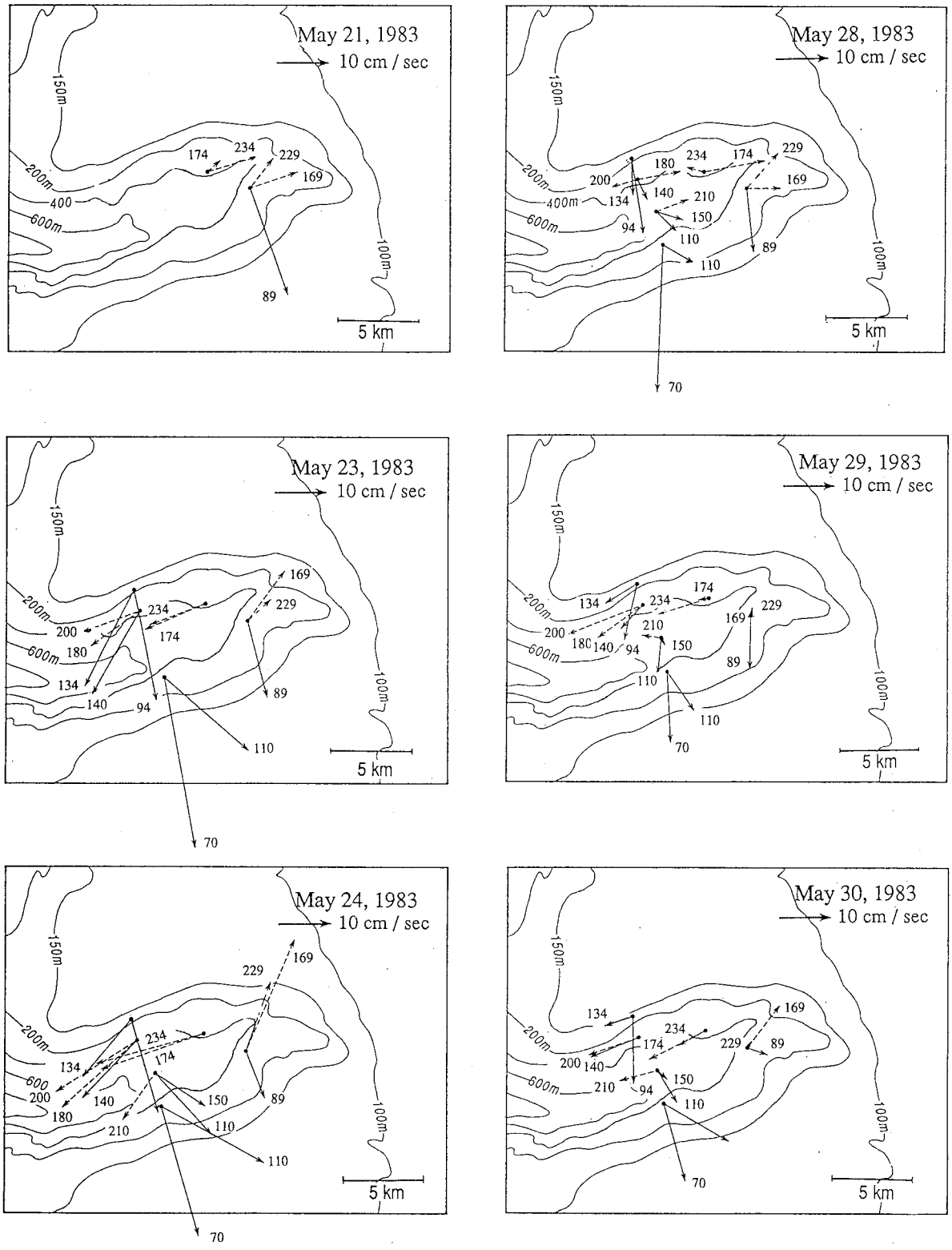

FIG. 8. Maps of vector velocity for selected upwelling events (maximum upwelling on 21 May, 28 May, and 8 June) and one downwelling event (maximum downwelling on 18 June). Measurement depth in meters is indicated near the tip of each vector. Locations above (below) the depth of the canyon rim are shown as solid (dashed) arrows.

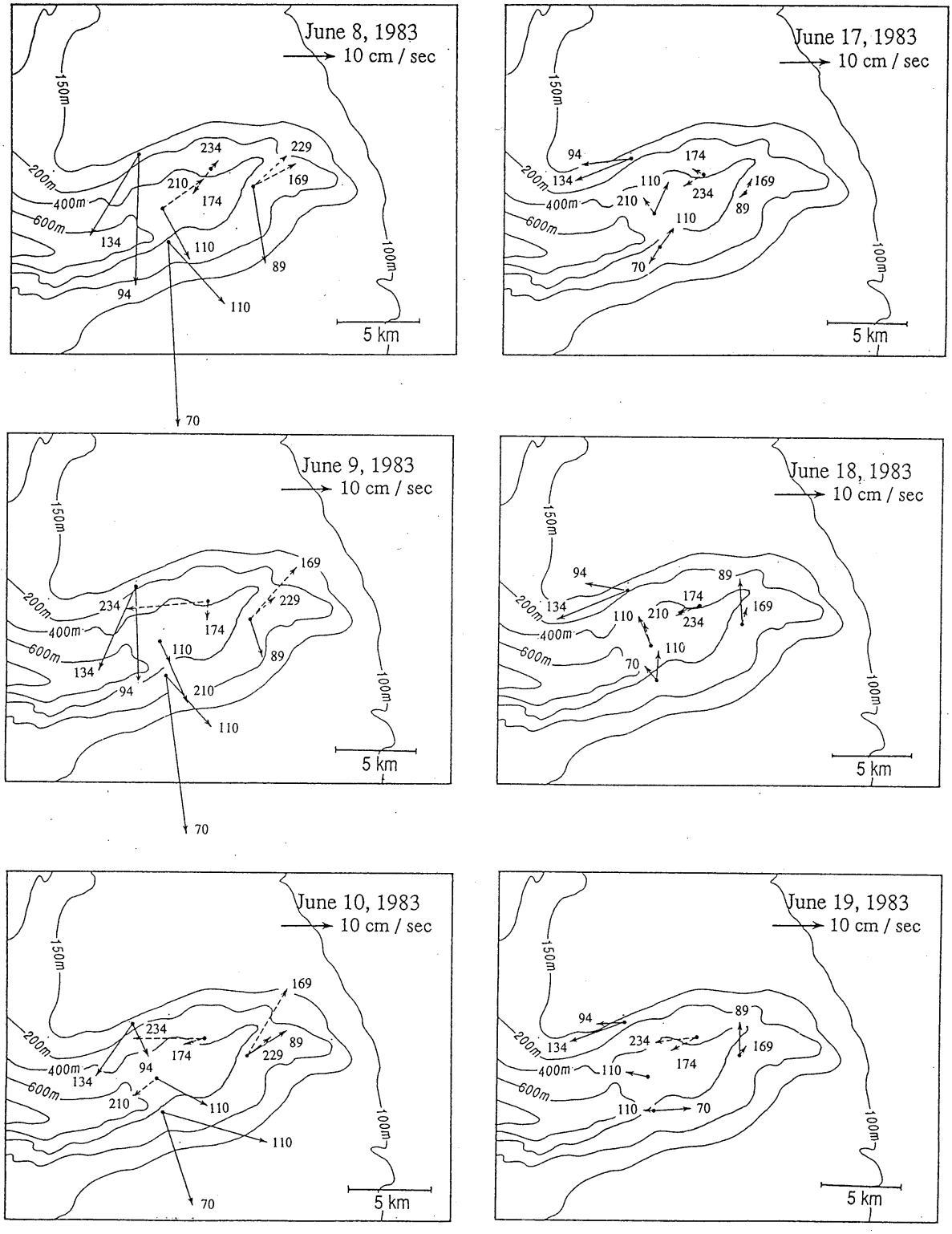

FIG. 8. (*Continued*)

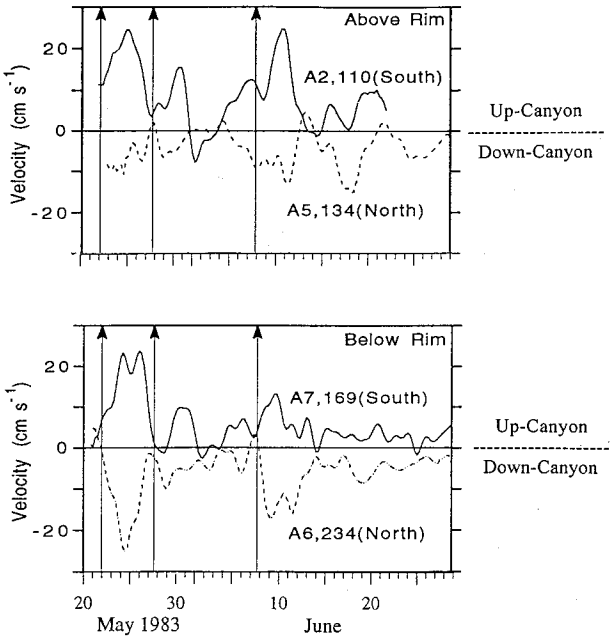

FIG. 9a. Time series of the east–west component of velocity at selected sites on opposite sides of the canyon above the rim (upper panel) and below the rim (lower panel). The data illustrate the increase in cross-canyon shear between or following minima in canyon temperature as indicated by the vertical arrows (i.e., upwelling). Up-canyon (i.e., eastward) flow is positive; down-canyon (westward) flow is negative.

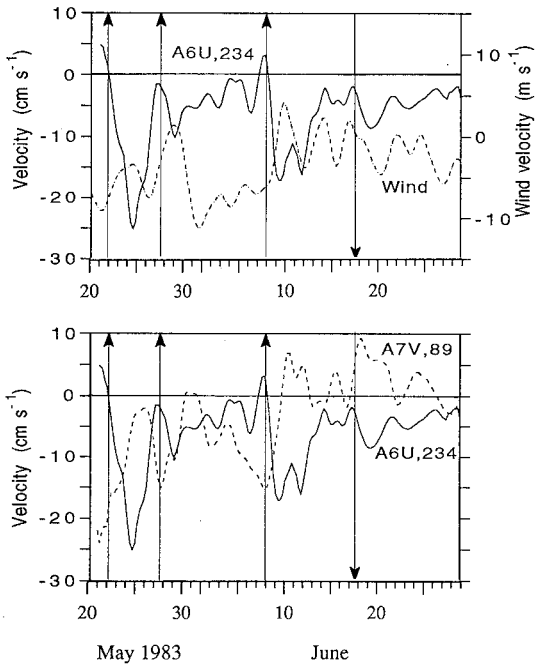

FIG. 9b. Up- and down-canyon velocity below the canyon rim (as indicated by the east–west component of velocity at A6 at a depth of 234 m (A6U, 234) versus alongshelf wind (upper panel) and velocity incident on the canyon (A7V, 89) (lower panel). Positive velocity is up-canyon (A6U) or northward (A7V and Wind).

(representing the canyon-specific flow field), leading it by roughly two and a half days.

To allow detailed comparison with actual bottom topography, EOF results are displayed on a bathymetric map constructed during the CTD surveys. The direction of flow below the canyon rim at the moorings on the canyon walls are clearly guided by very local topographic variations (see first EOF in Fig. 10).

6. Hydrographic variability and vertical velocity field

a. Fluctuations at individual sites

Time series of temperature at depths ~50 m above and at two depth intervals below the canyon rim (~50–100 m and >200 m) as well as near the rim are presented in Fig. 11a. In both depth intervals below the canyon rim, the data indicate a remarkably synchronous and spatially uniform response to the principal upwelling events. Spatial differences, which might be important to the dynamics, are masked in this figure by zero order upwelling effects. For example, close inspection of the figures reveals that minimum temperatures occur somewhat earlier (~0.5 d) at deeper sensors than at mid-depths (Fig. 11a, right panels). Note that the vertical arrows in all figures correspond to the deeper temperature minima. The amplitude of the fluctuations decreases with depth. However, the principal upwelling events are still detectable at the site 10 m above the canyon floor (570 m).

Time series of temperature at locations ~50 m above the canyon rim are also reasonably synchronous (Fig. 11a, upper left). However, the relationship of temperature extrema to the upwelling events is significantly different from that at locations below the canyon rim. In particular, the coldest water is often observed prior to that within the canyon or even between the apparent strong canyon cold water events.

The amplitude of temperature fluctuations just above and below the canyon rim are roughly similar, although they are not synchronous. Fluctuations at depths near the canyon rim, on the other hand, are much smaller than those either above or below the rim (Fig. 11a, lower left). Temperatures near the rim remain in the range 7.0°–7.5°C throughout the period considered.

Temporal relationships between fluctuations at selected depths throughout the entire water column are illustrated more clearly in Fig. 11b. The principle upwelling and downwelling events are marked with vertical lines. As described above, dominant signals above and below the rim are almost out of phase—rapid warming occurs above the canyon just following the occurrence of coldest water below the canyon rim. On the other hand, temperature fluctuations 70 m above the canyon rim show no similarity with fluctuations at any other depth.

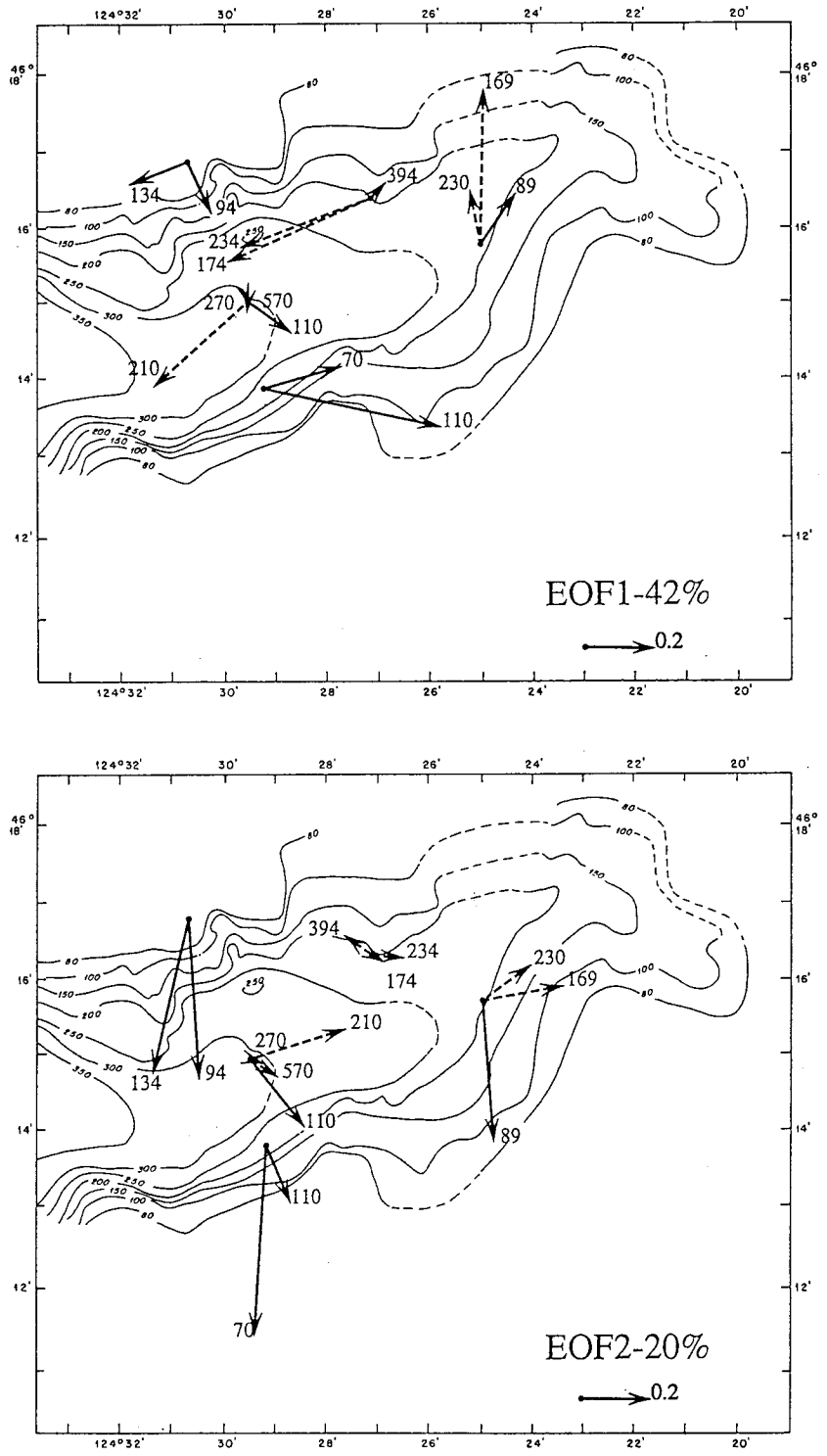

FIG. 10. Amplitude of the first and second EOFs of the velocity field within and over Astoria Canyon. EOFs were computed for the period 23 May–11 June 1983, corresponding to calculations for the means shown in Fig. 7. Locations above (below) the depth of the canyon rim are shown as solid (dashed) arrows. Measurement depth in meters is indicated near the tip of each vector. The smaller scale topographic map was produced from bathymetric data obtained during the Astoria studies.

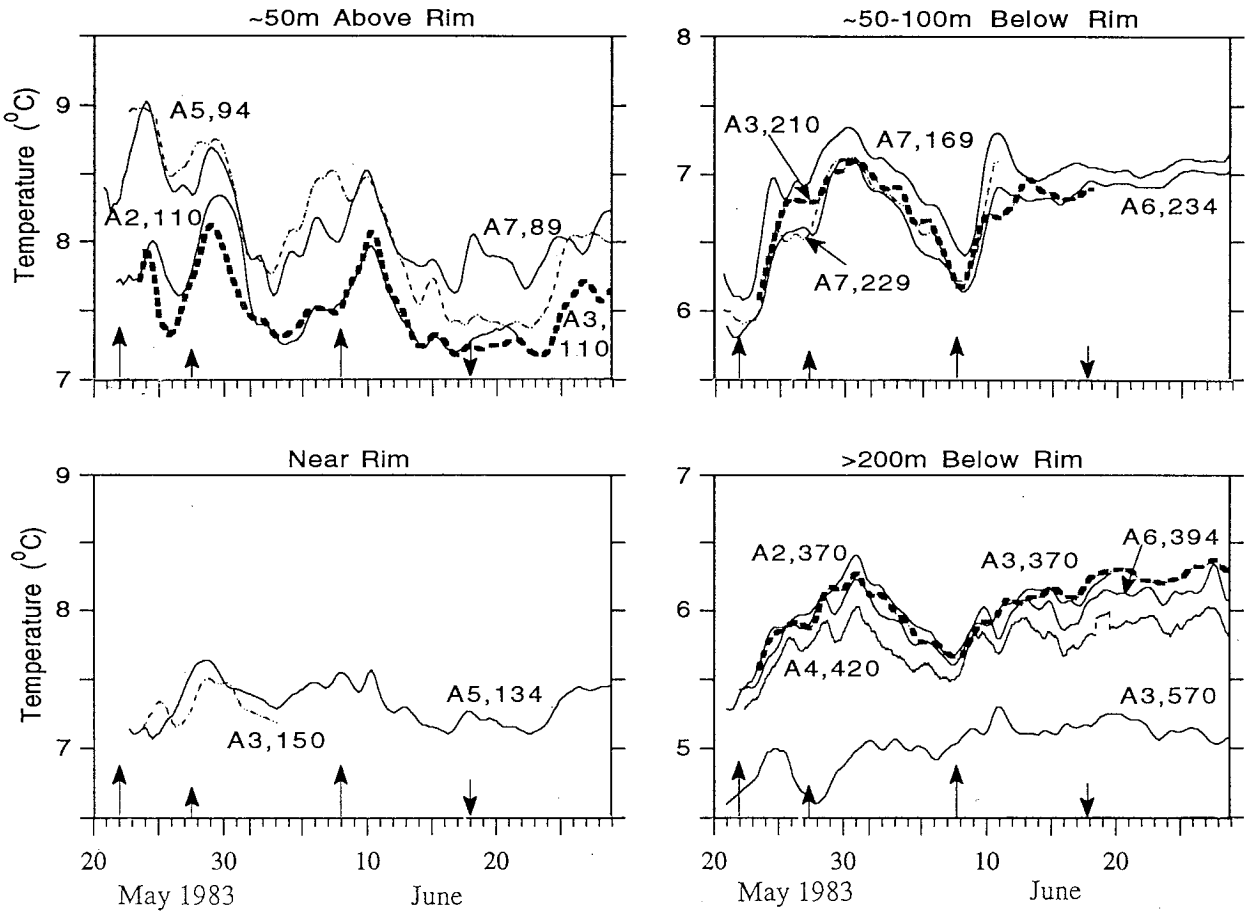

FIG. 11a. Time series of subtidal temperature in selected depth intervals relative to the depth of the canyon rim. Vertical scales are the same in all panels.

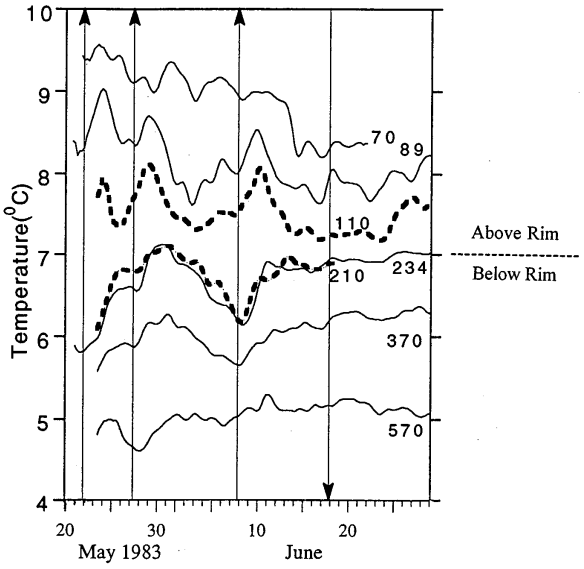

FIG. 11b. Time series of temperature at selected depths throughout the water column. With the exception of the data at 70 m (A2), 89 m (A7), and 234 m (A6), all data are from the mooring on the canyon axis (A3).

b. Two-dimensional structure

1) SURVEY SECTIONS

A contoured temperature section obtained from a CTD survey across the canyon on 21 May, just prior to maximum upwelling, is shown in Fig. 12a. The most striking features are a region of near constant temperature over the northern half of the section and a wedge-like region between the 6.0° and 6.5°C isotherms. Both of these characteristics result in a highly nonlinear vertical temperature gradient within 100–200 m of the canyon rim at most sites. On the following day, at the height of the upwelling event (as determined by the occurrence of the coldest water in the moored temperature time series below 300 m), the temperature wedge is still present, but the constant temperature region has disappeared or, alternatively, is not present at this location nearer the head of the canyon (Fig. 12b). A section at the head of the canyon the same day is remarkable in that the temperature structure is very similar to that at the more seaward location; that is, no evidence of enhanced upwelling near the canyon head is observed (Fig. 12c).

During an upwelling event water is displaced upward

within the canyon. At the same time, since the wind forcing and consequent upwelling are relatively large scale (~500 km; Halliwell and Allen 1987), upwelling and upward displacement of layers also occurs from the slope onto the shelf upstream of the canyon, and the water in these freshly upwelled layers is incident on the canyon along its upstream side and also at its seaward entrance. Because vertical displacement occurs both within and outside the canyon, temperature alone is insufficient to differentiate between newly upwelled canyon water and water that has come from upstream of the canyon. A better indicator of shelf water, one that allows it to be unequivocally separated from upwelling canyon water, is turbidity. A thin bottom boundary layer exists over the shelf, and this layer provides the only source of water of high turbidity over the canyon. Thus, the location of an intermediate nepheloid layer over the canyon provides a definitive separation of canyon and shelf water.

Attenuation data on 21 May provide dramatic evidence that the water in the uniform temperature layer on the north side of the canyon is shelf water that has recently dropped into the canyon (Fig. 12a). Sharp property gradients at both the top and bottom of the layer, as indicated by vertical profiles, are consistent with the fact that this layer has only very recently been displaced from its source (Fig. 12a, inset panel). Both attenuation and temperature layers shoal and thin from the north side of the canyon toward the south side. Attenuation contours (e.g., 0.6 m^{-1}) almost pinch off on the south side of the canyon axis and a similar structure is observed in the temperature field. Using the 0.6 m^{-1} attenuation contour as a tracer, we conclude that on 21 May, shelf water is confined roughly above the 7.0°C isotherm.

The nepheloid layer is generally thicker and occurs above the canyon rim on 22 May at the time of maximum upwelling along line 2 (centered at ~100 m vs 150 m on the previous day on line 1) (Fig. 12b). Shelf water is confined above the 6.5°C isotherm at this time and location. The nepheloid layer structure across the head of the canyon (line 3) is very similar to that at the more seaward location at that time (Fig. 12c). Note that although the water column below 200 m is more turbid than that on more seaward sections, the region bracketing the canyon rim (between ~100 and ~200 m) shows no evidence of enhanced turbidity at the head of the canyon.

2) SECTIONS FROM MOORED ARRAY

To investigate the temporal variability of both the thickness and vertical movement of layers below the canyon rim, we next examine selected time series of contoured temperature sections across the canyon. Individual layers are shaded in the figures to allow comparison of layer thickness and layer displacement over time (Fig. 13). The moored array data, in contrast to the CTD data, have been filtered to remove tidal effects. To obtain sufficient cross-canyon and vertical resolution, the assumption was made that cross-canyon gradients are much greater than along-canyon gradients and data from the two mooring transects were incorporated into one section. This assumption was based on the observation that no systematic along-canyon differences were found in temperature time series (see Fig. 11a). Data from moorings A6 and A7, north and south of the canyon axis, respectively, were placed in the same bottom depth as the mooring depth at the actual mooring site, because velocity data indicate that flow within the canyon over the walls is primarily along-isobath (see Fig. 10). These assumptions resulted in improved resolution on the two sides of the canyon where the CTD data showed the temperature field to be most nonlinear, that is, where linear interpolation over large vertical distances would result in the greatest error. Note that the regions above the canyon and near the lip are still poorly resolved in the resulting sections due to the nonlinearity of vertical temperature gradients in those regions.

The time series of the contoured temperature sections are consistent with large and rapid vertical movement of isotherms within the canyon during and following each upwelling event and each downwelling event (Fig. 13). For example, the 6.5°C isotherm is at the canyon rim on 23 May immediately following the first upwelling event but drops to a depth of 250 m just two days later. The 7.0°C isotherm is centered at ~280 m on 29 May but is above the canyon rim on the south side (~140 m) on 6–8 June during the second major upwelling event. During the weak downwelling event (18–19 June), isotherms below the canyon rim remain relatively fixed while isotherms above the canyon move downward over the south half of the canyon between 18 and 19 June.

The contoured temperature sections also suggest that rapid changes in layer thickness occur over time. Layers moving upward toward the canyon rim during upwelling are compressed (e.g., the 6.5°–7.0°C layer on 21–23 May and on 8 June during upwelling is much thinner than on 25 May following upwelling or on 4 June preceding upwelling) while those deeper in the canyon are stretched (e.g., the 5.0°–5.5°C layer is much thicker on 23 May and on 8 June during upwelling than prior to or following upwelling). In the following sections the contoured temperature data are used to provide explicit estimates of both the vertical velocity and layer thickness as a function of time.

c. Vertical velocity

With the assumption that mixing is negligible, the time rate of change of temperature is governed by the relationship

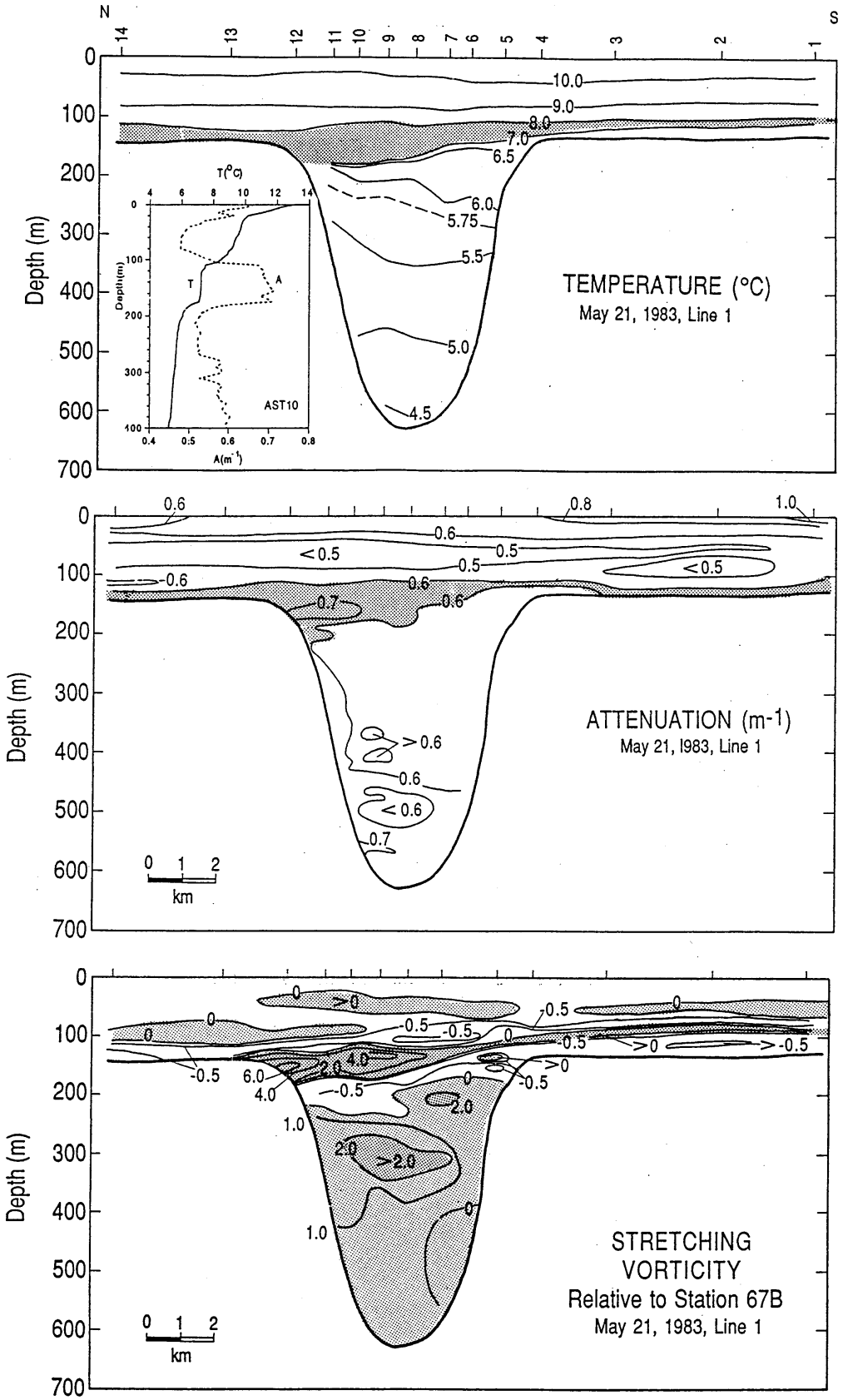
N
S
14 13 12 11 10 9 8 7 6 5 4 3 2 1
Depth (m)
10.0
9.0
8.0
7.0
6.5
6.0
5.75
5.5
5.0
4.5
T(°C)
Depth(m)
T
A
AST10
A(m⁻¹)
TEMPERATURE (°C)
May 21, 1983, Line 1
0.6
0.8
1.0
<0.5
0.5
0.7
>0.6
ATTENUATION (m-1)
May 21, 1983, Line 1
0 1 2
km
>0
-0.5
2.0
4.0
6.0
1.0
STRETCHING
VORTICITY
Relative to Station 67B
May 21, 1983, Line 1

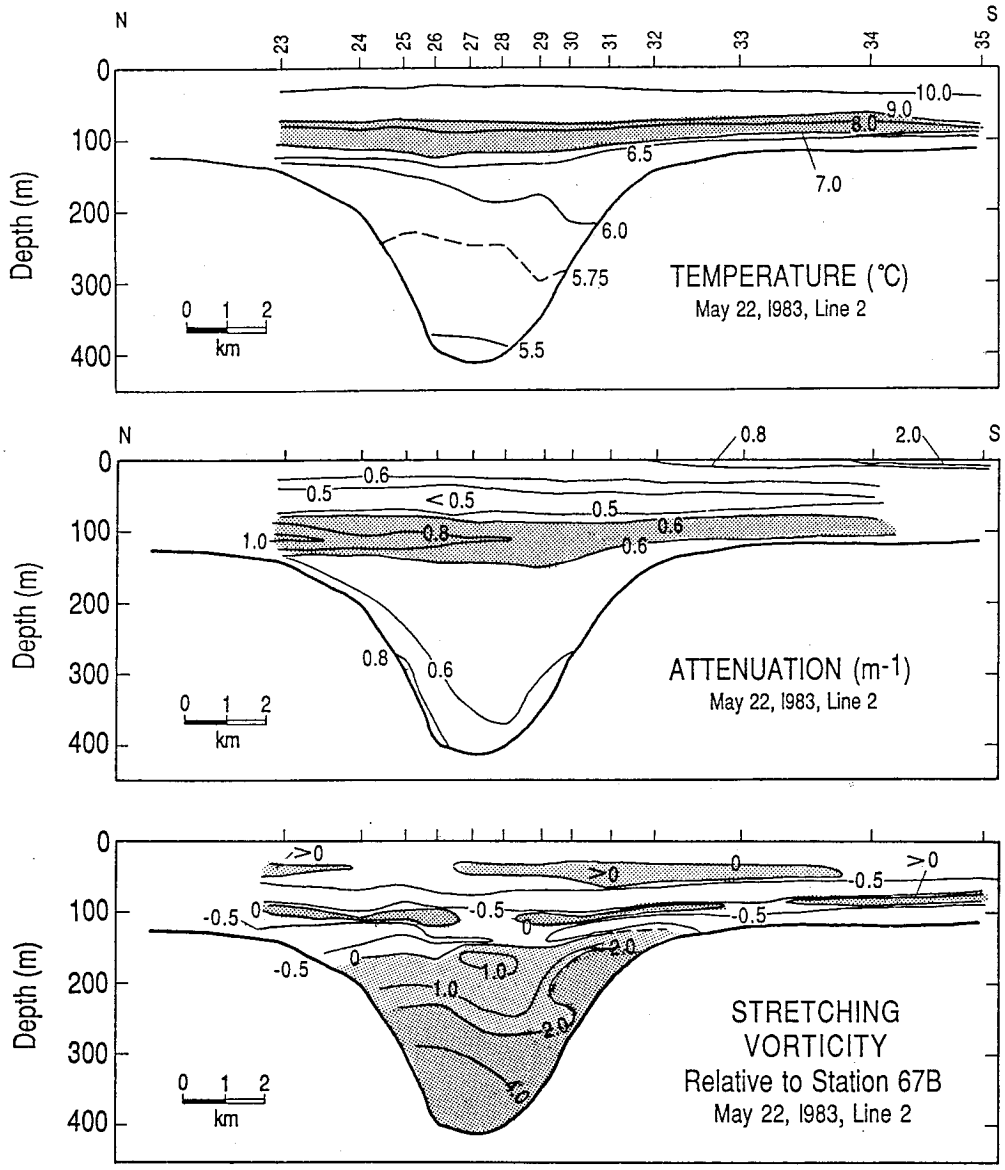

FIG. 12b. Contoured sections of temperature, attenuation, and stretching vorticity on line 2 (midcanyon) across Astoria Canyon on 22 May. Location of the section is shown in Fig. 1.

$$\frac{\partial T}{\partial t} = -u\frac{\partial T}{\partial x} - v\frac{\partial T}{\partial y} - w\frac{\partial T}{\partial z}, \tag{1}$$

where u, v, and w are the east–west (positive eastward), north–south (positive northward), and vertical (positive downward) components of velocity. Note that the assumption of negligible mixing may not be valid near the head of the canyon where enhanced internal wave activity is likely (Hotchkiss and Wunsch 1982). If lateral advective gradients are small, then (1) reduces to

$$\frac{\partial T}{\partial t} = -w\frac{\partial T}{\partial z}. \tag{2}$$

Ideally, one could demonstrate the insignificance of lateral advection using direct estimates from the dataset.

←

FIG. 12a. Contoured sections of temperature, attenuation, and stretching vorticity on line 1 across Astoria Canyon on 21 May. Location of the section is shown in Fig. 1. Vertical profiles of temperature and attenuation at station 10 are shown as an inset. Note the thermostad (the region of near-constant temperature) near the depth of the canyon rim.

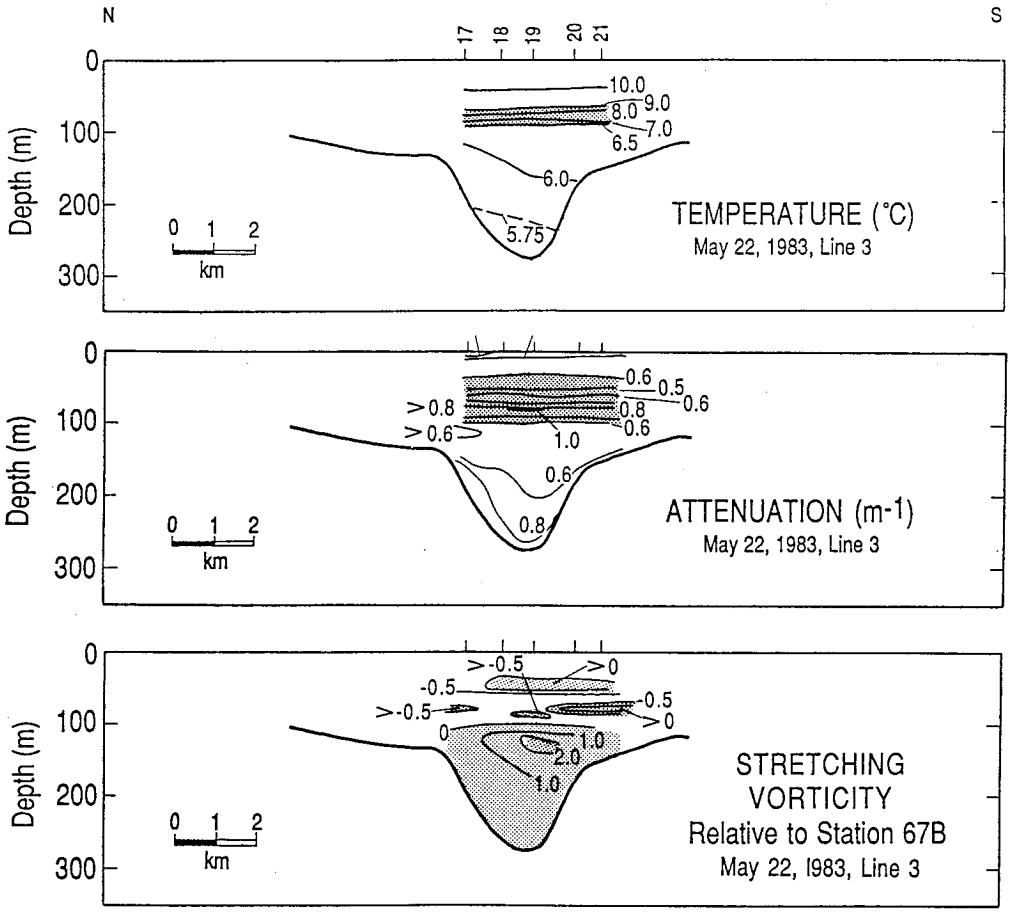

FIG. 12c. Contoured sections of temperature, attenuation, and stretching vorticity on line 3 (at the canyon head) across Astoria Canyon on 22 May. Location of the section is shown in Fig. 1.

Unfortunately, with the relatively large measured velocities (~10 cm s^{-1}), relatively small temperature differences (~0.1°–0.2°C) produce advective temperature changes comparable to the observed temperature changes. However, the spatial temperature differences are within the uncertainty produced by sensor depth and sensor location relative to canyon topography. At the one depth for which a reasonable estimate could be obtained (A3, 210 u velocity, using A7, 234 − A3, 210 for the temperature difference), $u(\partial T/\partial x)$ was about 10% of $\partial T/\partial t$. For most data pairs the sign of the advective terms mirror the velocity field used to compute the gradient. Since the lateral velocity field has significant spatial gradients and is frequently in opposite directions at different sites (see velocity maps in Fig. 8 and EOF results in Fig. 10), it seems unlikely that lateral advection could account for the spatially homogeneous temperature signal observed in the canyon. For example, as upwelling subsides and flow on the two sides of the canyon is in opposite directions, the lateral temperature gradients must have the opposite sense on the two sides of the canyon to produce a spatially uniform temporal gradient in the canyon. Because this seems highly unlikely, we assumed that the dominant temperature changes over time are due to changes in vertical velocity. Send et al. (1987) had similar difficulties in obtaining estimates of lateral temperature gradients over the California shelf using data from the relatively dense CODE array. They also resorted to patterns of variability to argue that certain terms could be neglected. Similarity between the computed upwelling rates and model results (see section 8) and between time series of vertical velocity and relative vorticity as well as alongshelf wind (see section 7) provide a priori confirmation that this assumption was reasonable.

1) BELOW THE CANYON RIM

To obtain the best possible estimates of vertical velocity, temperature gradients were computed (following linear vertical interpolation) over excursions during about one-half day (~20 m) above and below the height at which the time gradient was calculated. Estimates at different sites were similar in important details. Only one example (A6, 234) is reported here, and no attempt was made to average results. Vertical velocity estimates

relative to both the alongshelf component of wind and the velocity incident on the canyon are shown in Fig. 14a. Note that the ~0.5 d mismatch between the position of the vertical arrows indicating minimum temperature and the occurrence of zero vertical velocity is due to the fact that temperature minima occur about 0.5 d earlier at ~400 m (signified by the arrows) than at ~230 m (where vertical velocity was calculated). Vertical velocity is significantly correlated with alongshelf wind ($r = 0.6$) with no significant lag over the record. The strong correlation, obtained in spite of the fact that wind estimates were from calculated rather than measured wind, suggests that the assumptions used to estimate vertical velocity were not unreasonable. The phase relationship between wind and vertical velocity is consistent with wind-forced coastal upwelling; that is, southward wind (and hence wind stress) is associated with upwelling, and northward wind or minima in southward wind are associated with downwelling or with minima in upwelling velocities. Upwelling rates approach 50 m d^{-1}. Downwelling rates during the relaxation following the upwelling often exceed upwelling rates by as much as a factor of 2 (up to 90 m d^{-1}).

The relationship between vertical velocity and alongshelf incident flow is much weaker than that with alongshelf wind (Fig. 14a, right panel). In general, extrema in vertical velocity *precede* extrema in incident flow. Although maximum upwelling velocity *leads* maximum incident southward velocity by less than 0.5 d, the phase lag is much more pronounced for the several maxima in northward flow (or minima in southward flow), vertical velocity leading incident flow by 1–3 d. Note that the weak relationship with incident velocity does not appear to be due to the choice of the time series used as a proxy for the incident flow field. The relationship of vertical velocity with flow at similar depths at canyon sites other than that used for the incident flow as well as at the Oregon midshelf site is much weaker than that displayed in Fig. 14a (not shown).

2) ABOVE THE CANYON RIM

As previously discussed, temperature fluctuations at stations just above the canyon (within ~50 m of the rim) are also relatively synchronous at the several canyon sites (see Fig. 11a). However, these fluctuations differ from those within the canyon and also from those at locations closer to the surface. The temperature fluctuations *above* the canyon rim are well correlated with and in phase with both the vertical velocity *below* the rim and alongshelf wind (coldest temperature, maximum upwelling, and maximum southward wind being roughly coincident), but are not strongly related to incident flow (Fig. 14b). The correlation with wind extends beyond the several strong upwelling events at the beginning of the records that have been emphasized in our analysis (Fig. 14b, lower panel). The robust relationship between temperature *above* the canyon and vertical velocity *within* the canyon implies that coldest temperatures occur above the canyon when upwelling within the canyon is a maximum. Since upwelling continues within the canyon after vertical velocity is a maximum (although at a reduced rate), these results suggest that upwelled water exits the canyon laterally rather than vertically during the relaxation phase of the upwelling event.

d. Layer thickness

As previously mentioned, at the time of maximum upwelling, the upwelling of layers from within the canyon results in layer compression near the canyon rim (Figs. 12a,b and 13). Deeper in the canyon, layers are stretched during upwelling. For example, note the change in thickness of the 5.0°–5.5°C layer between 23 and 24 May as upwelling declines and between 4 and 8 June as upwelling increases (Fig. 13a).

To quantify changes in layer thickness, layer thicknesses were measured at the middle and on the north and south sides of the canyon (near moorings 6 and 7, respectively) from the contoured sections shown in Figs. 12 and 13 (only a subset is shown in the figures). The three layer thicknesses for each date were then averaged for each layer to obtain average layer thickness. The thickness of selected temperature layers, on average, over the canyon (7.0°–7.5°C) and within the canyon (5.5°–6.0°C) are presented in Fig. 15. The figure illustrates that each layer thickness has its own distinct time history, a function of the various processes that act to compress or stretch it at whatever depth and location the layer resided at each instant. Both shallow and deep layers change thickness by at least a factor of 2 during the two dominant upwelling events; the shallowest layer compresses; whereas, the deepest layer stretches. In the following section, time series of layer thickness are compared with estimates of relative vorticity calculated from the moored array velocity field.

7. The vorticity field

a. Spatial variability

Conservation of potential vorticity for inviscid flow requires that when layers are stretched or compressed, relative vorticity is increased or decreased, respectively. Consider a layer of thickness h that is stretched to a thickness h_c as it flows over the canyon. By conservation of potential vorticity, and assuming that upstream relative vorticity is negligible, then

$$\frac{f}{h} = \frac{f + \mathrm{RV}}{h_c}, \tag{3}$$

where RV is relative vorticity $\partial v/\partial x - \partial u/\partial y$. The assumption of negligible upstream vorticity is reasonable for a typical upwelling jet over the outer shelf and upper

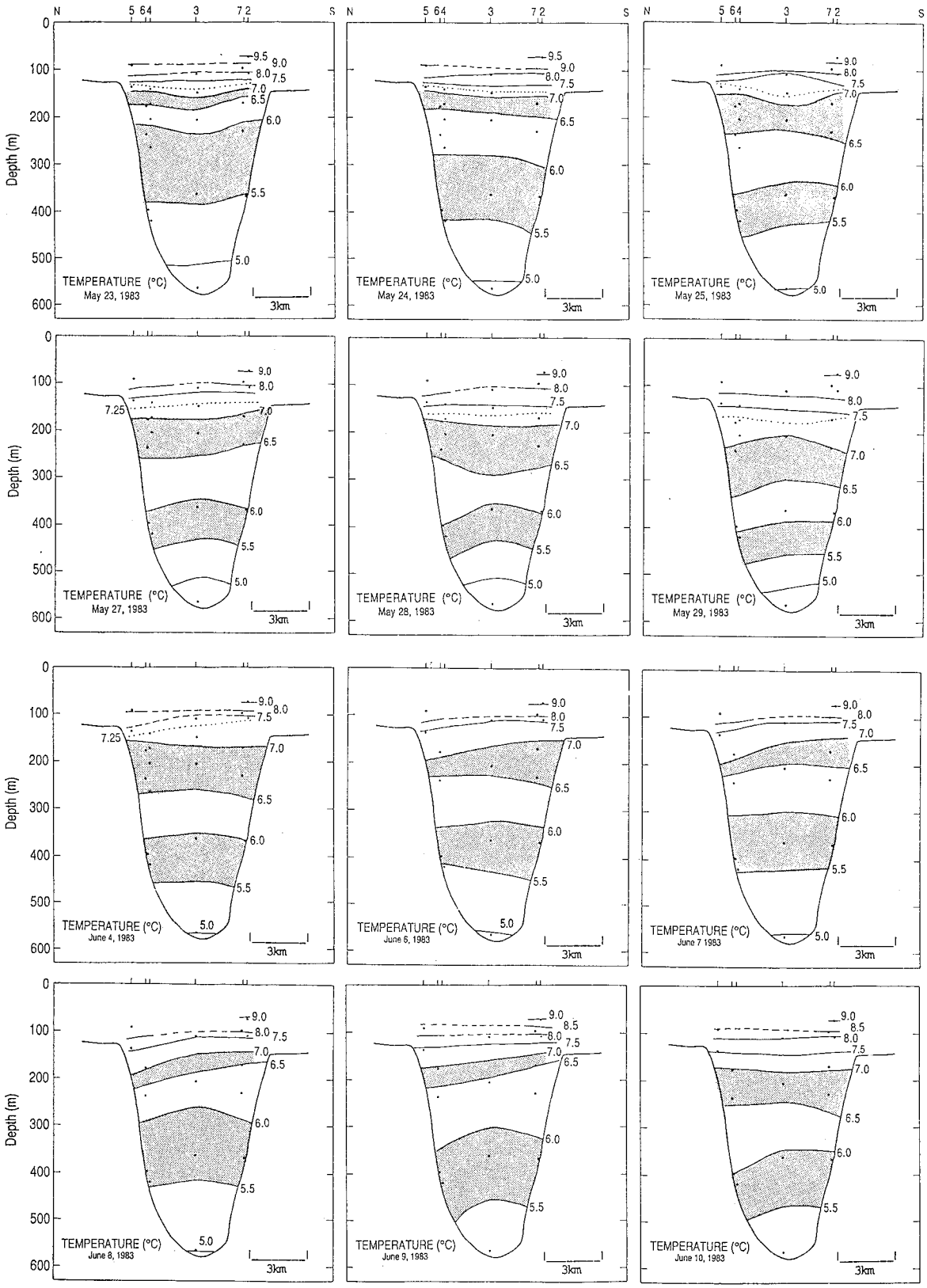

FIG. 13. Time series of contoured temperature sections including the several upwelling events and one downwelling event discussed in the text. Contours were obtained from the moored array data and sensor locations are shown as dots. Dashes are used to indicated speculative contours. Dots are used for the 7.25°C contour. To facilitate monitoring of layer thickness and depth the same temperature layers are shaded in all sections.

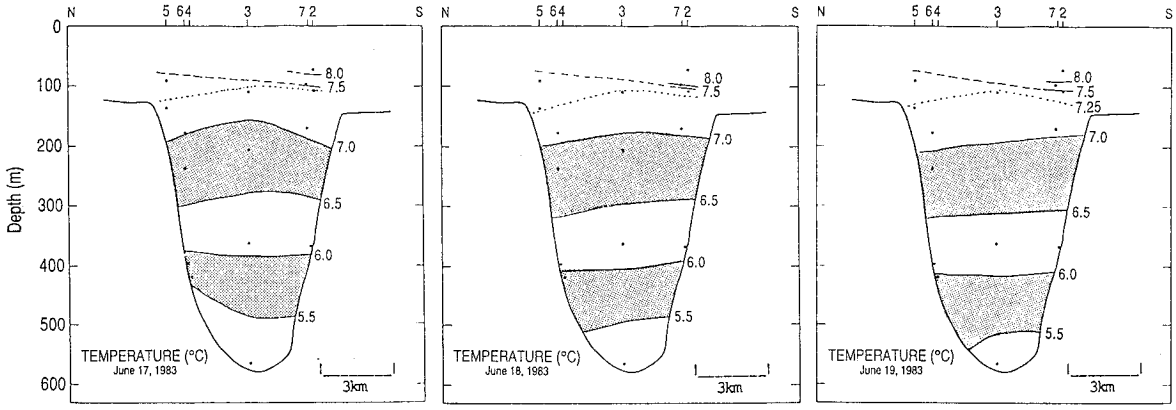

FIG. 13. (*Continued*)

slope, for which RV $\sim 0.1f$ (Allen 1996). Rearranging terms in (3), we have, for each flow layer,

$$\left(\frac{h_c}{h} - 1\right) f = \text{RV}. \tag{4}$$

The left-hand side of (4) is often referred to as stretching vorticity (SV).

The preceding discussions suggest that layers may be stretched downward as they fall into the canyon. At the same time, upwelling from the canyon during an upwelling event results in layer compression at the top of the canyon and stretching throughout the rest of the canyon. To attempt to quantify the potential vorticity generated by such processes, stretching vorticity was estimated from layer thicknesses derived from the contoured temperature sections shown in Fig. 13. The calculation was performed on individual temperature layers at 0.25°C intervals from 5.0° to 8.0°C, at 0.5°C intervals from 8° to 10°C, and at 2°C intervals for temperatures exceeding 10°C. More resolution is required in deeper layers where the vertical temperature gradient is smaller.

The choice of an upstream layer thickness (h) condition is not straightforward. Layers over the canyon and within the canyon have different sources, one from the upstream shelf, the other from the offshore slope. Moreover, upstream conditions vary with time even during a single upwelling event. Further limitations on possible choices occur because this is an El Niño year. The upper water column off the coast was substantially altered by the El Niño; temperatures were as much as 2°C warmer than average at the sea surface, 0.5° warmer at 300 m, and 0.2°C warmer at 500 m (Cannon et al. 1985; Tabata 1985). Several hydrographic sections were obtained off Washington and Oregon in 1982 and 1983 to study El Niño effects in the Pacific Northwest. Fortuitously, one section was obtained about 100 km north of Astoria Canyon only two days prior to the first hydrographic section in the Astoria study (Reed 1984). Time series in Huyer and Smith (1985) illustrate that upwelling was already very strong at this time—this event marks the primary spring transition in 1983. The station in the Reed data closest to the Astoria shelfbreak depth is station 67B, located on the north side of the very narrow Grays canyon. For layers deeper than the bottom depth of station 67B we have used data from the next seaward station (67C). This choice is reasonable if flow at deeper depths enters the canyon from the adjacent slope area.

The spatial pattern of the resulting estimates of stretching vorticity is consistent with the qualitative discussion of the stretching/compression of flow layers. In particular, on 21 May along line 1, there is a remarkable correspondence between the location and structure of the intermediate nepheloid layer over the canyon and the location of a region of strong cyclonic vorticity (Fig. 12a). Stretching vorticity in this layer is as high as $6f$. Cyclonic vorticity occurs throughout most of the deeper canyon, with a maximum of about $2f$. A thin layer of anticyclonic vorticity ($< -0.5f$) occurs between the two regions of cyclonic vorticity and another occurs just above the cyclonic layer that emanates from the upstream canyon rim (Fig. 12a, lower panel). On 22 May along line 2 at maximum upwelling the maximum in turbidity also coincides with a layer of minimum anticyclonic or weak cyclonic vorticity. Also, cyclonic stretching vorticity is observed at deeper depths and is separated from the near rim cyclonic layer by a thin region of anticyclonic vorticity, as on 21 May on line 1 (Fig. 12b). The stretching vorticity pattern on line 3 at the head of the canyon is very similar to that for the midcanyon section on the same day (Fig. 12c). These results suggest that layers can be stretched in several ways during an upwelling event: they may fall into the canyon (as on 21 May) or stretch gradually as they flow over the canyon (as on 22 May); alternatively, layers deeper in the canyon are stretched as they are upwelled through the canyon.

To examine the sensitivity of the above results to upstream conditions, estimates of stretching vorticity were obtained using other available data for upstream

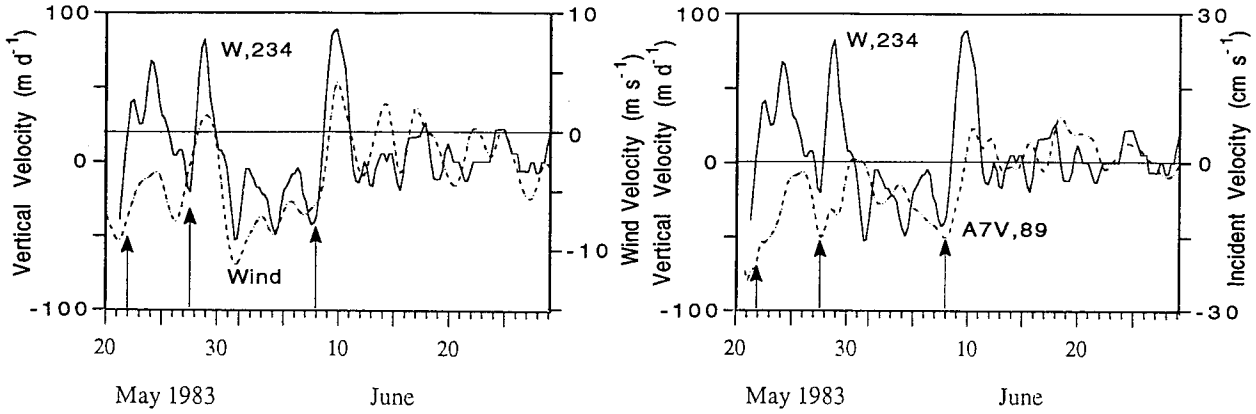

FIG. 14a. Time series of vertical velocity below the canyon rim (*W*, 234) versus alongshelf wind (left panel) and incident velocity (A7V, 89) (right panel). Vertical velocity is positive downward; wind and incident velocity are positive northward.

conditions, including a monthly mean and upwelling events in May and June 1982 and in early May 1983. The monthly mean temperature profile was calculated from all available data (10–20 per month) off Washington and Oregon over the continental slope (300–800 m; 45°–46.5°N, 124.4°–125°W). Comparison of the results obtained from these various datasets with the results presented above demonstrated that, although the magnitude of stretching vorticity estimates can vary by almost an order of magnitude depending on the choice of initial layer thickness, the principal spatial patterns discussed above are robust (not shown). In every case examined, values of cyclonic stretching vorticity within the canyon were less than those obtained using the ''best available'' data. These sensitivity studies, combined with the unrealistically large values of stretching vor-

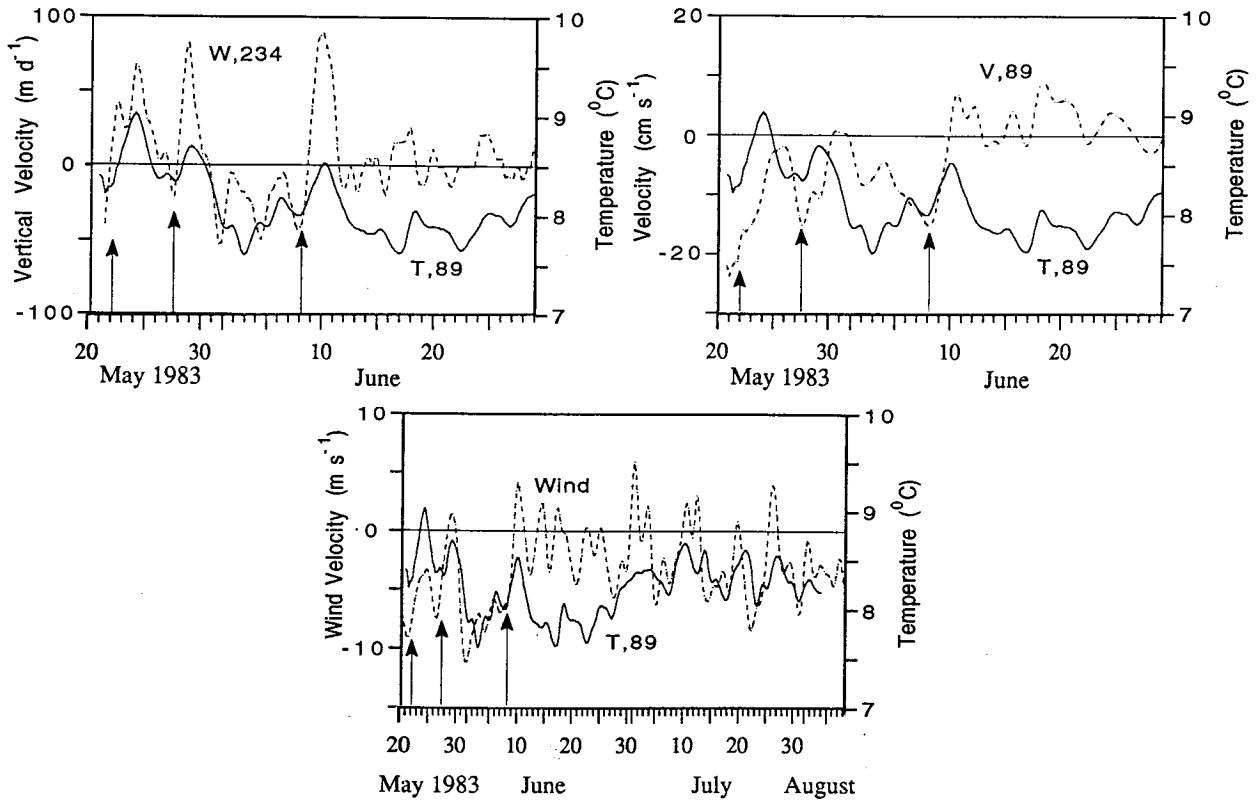

FIG. 14b. Time series of temperature at a location above the canyon rim (*T*, 89 m) versus vertical velocity *below* the rim (*W*, 234) (upper left), incident velocity (*V*, 89) (upper right), and alongshelf wind (lower panel). Note that the wind/temperature time series are shown for a longer time period than the other records.

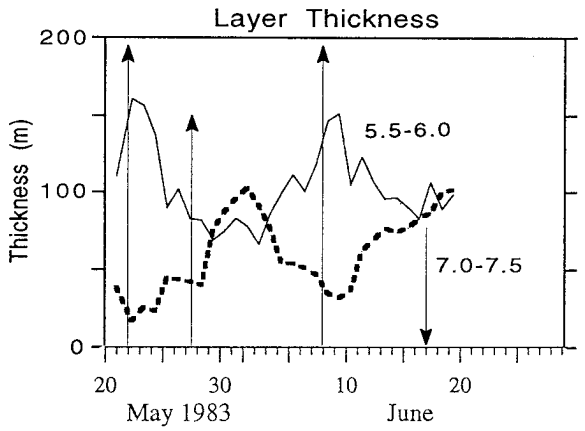

FIG. 15. Time series of individual layer thickness for layers that are always within the deep canyon (5.5°–6.0°C) and generally near the canyon rim (7.0°–7.5°C).

ticity estimated in regions near the canyon rim, suggest that the upstream layer thicknesses used in the calculations may underestimate the actual upstream layer thickness to some extent.

b. Temporal variability

Ideally, to demonstrate a link between layer stretching and canyon circulation, time series of stretching vorticity and time series of relative vorticity would be compared at selected sites. Unfortunately, no data are available to provide estimates of upstream vorticity and/or layer thickness except two days prior to the first upwelling event. At a fixed depth and location, a different layer is presented to the sensors from the moored array at each instant and the upstream thickness of that layer is unknown. Thus, it is not generally possible to estimate stretching vorticity from the moored array data. On the other hand, the *relative* vorticity field *can* be estimated from the moored array data. Given the large vertical shear in velocity at all sites, reasonable estimates of gradients were possible for only two depth intervals: ~40 m above the rim (RV, 110) and ~80 m below the rim (RV, 230).

1) BELOW THE RIM

At depths ~80 m below the canyon rim, cyclonic vorticity is significantly correlated to ($r = 0.5$) and in phase with vertical velocity in the same depth interval (Fig. 16a, upper left); during upwelling periods, cyclonic relative vorticity is a minimum and during downwelling periods, cyclonic vorticity is a maximum (Fig. 16a, middle left). The robust relationship provides confirmation that the assumptions used to estimate both vorticity and vertical velocity were reasonable. At the onset of each upwelling event, that is, when velocity incident on the canyon is a maximum, flow ~100 m below the rim is up-canyon at all sites and cyclonic vorticity is a minimum. Maximum cyclonic vorticity below the canyon rim, because it is coincident with maximum downwelling, occurs ~1–2 d after the temperature minimum at that depth (but before the temperature maximum; Fig. 16a, middle right) and ~1–3 d after the maximum southward incident velocity (but before the minimum southward velocity; Fig. 16a, upper right).

The temporal variability of the relative vorticity below the canyon rim is reasonably similar to that of average layer thickness of layers that are usually below the canyon rim (5.5°–6.0°C), suggesting that the changes in relative vorticity are related to the stretching and/or compression of layers that pass by the sensor (Fig. 16a, lower left). Taking the calculation one step further, the June monthly mean temperature profile was used for upstream layer depth and estimates of stretching vorticity were calculated. Both the magnitude and temporal variability of estimates of stretching vorticity so obtained are reasonably similar to the estimates of relative vorticity (Fig. 16a). Thus, we conclude that the stretching of layers via upwelling within the canyon is reasonably consistent with the observed increase in cyclonic vorticity that follows the upwelling. Maximum stretching and, hence, maximum vorticity occurs somewhat after the peak of the upwelling event as the layers drop back down into the canyon when the time rate of change of temperature (i.e., downwelling) below the rim is also a maximum.

The spatial pattern of stretching vorticity at maximum upwelling as obtained from the CTD sections suggests that a subsurface maximum in stretching vorticity occurs near 300–400 m (Figs. 12a,b). Also, time series of layer thickness for the deepest canyon layers are consistent with layer stretching during both the May and June upwelling events (see Fig. 13). Only two current meters were situated near these depths: A6, 394 and A3, 360. Estimates of relative vorticity obtained using these data are consistent with a relative maximum in cyclonic vorticity on 22 May (not shown). However, the magnitude of the relative vorticity ($0.2f$) is an order of magnitude less than the estimated stretching vorticity at these depths. Relative vorticity at these depths decreases after the May upwelling event and then begins to increase so that cyclonic vorticity is a maximum on 8 June at the height of the third upwelling event.

2) ABOVE THE RIM

Maximum cyclonic relative vorticity ~40 m *above* the canyon occurs 1–2 d later than that below the canyon rim, when the incident velocity field relaxes following the upwelling event; i.e., when the incident southward velocity is weakest, or even northward (Fig. 16b, top left). This suggests that the dynamics governing the flow above the canyon differ from those below the canyon. Maxima in cyclonic vorticity *follow* the above-canyon temperature maxima (Fig. 16b, top right). Thus, vertical velocity above the canyon (proportional to the time rate of change of temperature) is roughly *inversely* related to the relative vorticity (not shown). The time variability

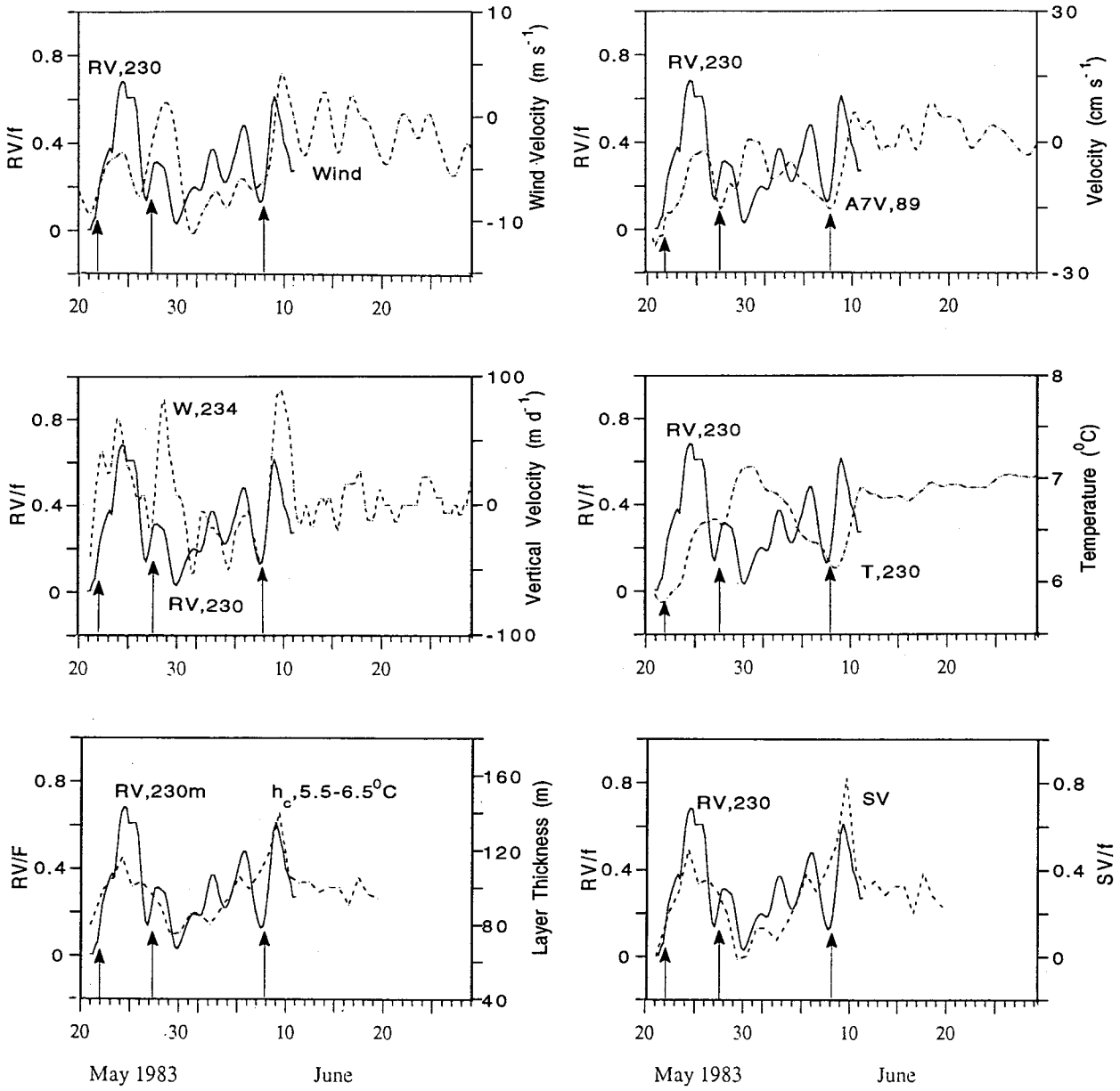

FIG. 16a. Time series of *relative* vorticity divided by f ~80 m below the canyon rim (RV, 230) compared with alongshelf wind, vertical velocity below the canyon rim (*W*, 234), incident velocity (A7V, 89), temperature below the rim (*T*, 230), average layer depth (h_c), and an estimate of stretching vorticity divided by *f*(SV). Vertical velocity is positive downward; wind and incident velocity are positive northward.

of the relative vorticity is reasonably similar to that of layer thickness, thickest layers being associated with maximum cyclonic vorticity (Fig. 16b, bottom).

To investigate these relationships in more detail, the turning angle of the flow in the upper water column was calculated at several depths and locations. Results were similar for all records. Turning angle (calculated with respect to due south) is closely related to relative vorticity (Fig. 17, middle panel). Comparison with the time-variable Rossby number of the incident flow illustrates that during the strongest upwelling, when incident flow and, hence, the Rossby number are large, turning angle is small; that is, the cyclonic circulation over the canyon appears to be suppressed (Fig. 17, upper panel). As the upwelling relaxes and the incident velocity decreases, the turning angle of velocity vectors increases, consistent with a cyclonic circulation pattern. The data suggest that a cyclonic pattern exists for Rossby numbers below about 0.25.

In spite of the absence of closed topographic contours, it is tempting to compare the cyclonic pattern above the canyon to a stratified Taylor column (Hogg 1973). Model studies indicate that the shape, height, and longevity

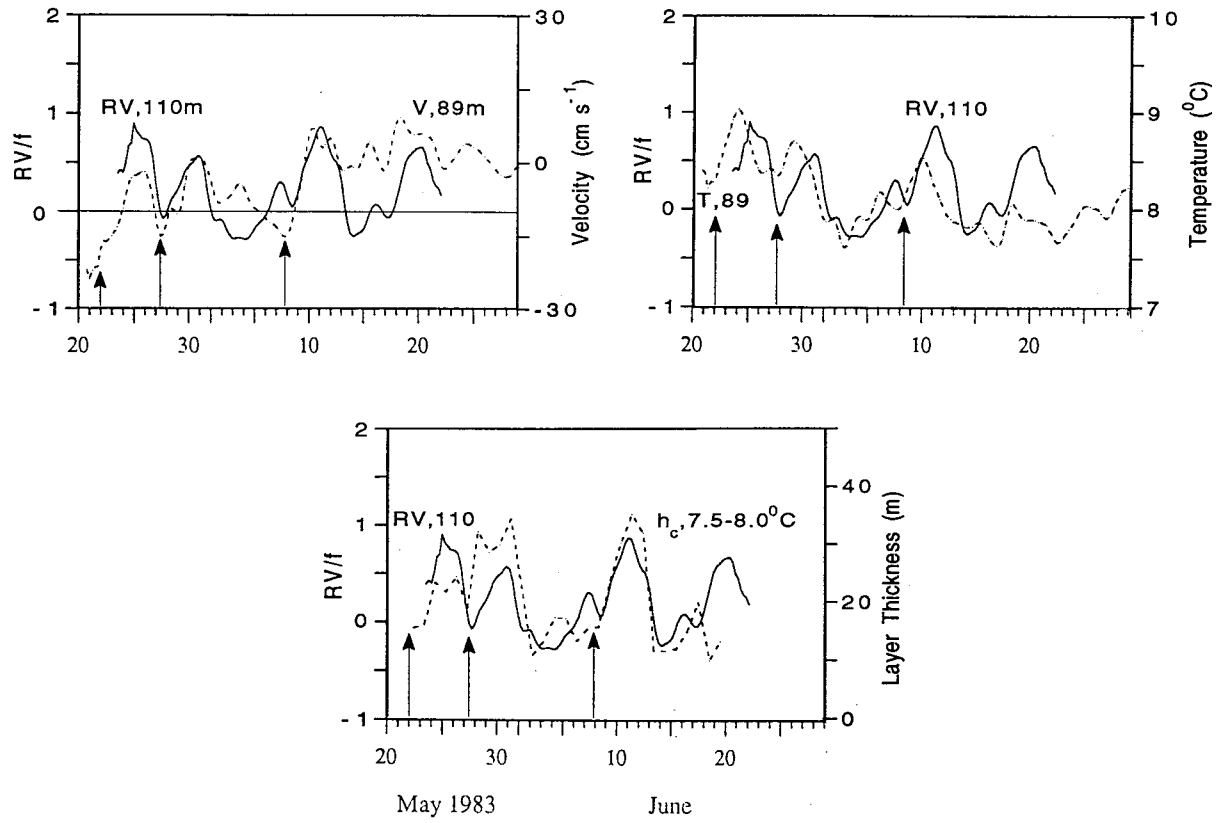

FIG. 16b. Time series of *relative* vorticity divided by f ~40 m above the canyon rim (RV, 110) versus incident velocity (V, 89), temperature at the same depth (T, 89), and average layer depth above the canyon (h_c).

of a Taylor cap is a function of incident flow, stratification, and the width of the feature as well as its aspect ratio (Huppert and Bryan 1976; Chapman and Haidvogel 1992). Chapman and Haidvogel (1992) predict that a Taylor cap should occur over a seamount for Rossby numbers below about 0.15.

The stratification in the Astoria observations is roughly an order of magnitude greater than that utilized in Chapman and Haidvogel (1992) and in most other papers that treat Taylor caps. Also, the stratification increases by a factor of 2 between the beginning and end of upwelling events. To investigate possible effects of this variability in stratification velocity, turning angles were plotted against the vertical stratification scale (Fig. 17, bottom panel). Vertical decay scales were on the order of 40–60 m during the upwelling events and 80 m between the events. No consistent temporal relationship between turning angle and stratification is observed. Nor did we observe the turning angle to change with height in a consistent way—turning angles at both 70 m and 110 m from the surface were generally in phase (not shown). Hogg (1973) demonstrates that, at least in the quasigeostrophic case, the height of a Taylor cap does not decrease indefinitely with increasing stratification; that is, a limiting thickness is reached.

3) NEAR THE RIM

Extremely large values of cyclonic stretching vorticity (up to 6f) were estimated prior to maximum upwelling using CTD data from the upstream side of the canyon near the rim (Fig. 12a). This layer of cyclonic vorticity appeared to be sandwiched between two layers of anticyclonic vorticity. Relative vorticity time series at depths of about 110 m and 230 m were consistent with minima in anticyclonic vorticity at this time (Figs. 16a,b). Is there any evidence in the relative vorticity field to support the existence of a *cyclonic* region near the rim at maximum upwelling? Unfortunately, no data are available from the moored array near the rim during the first upwelling event. However, data are available during the second event and these data (A4, 140 and A3, 150) do demonstrate cyclonic vorticity at maximum upwelling (28 May) when circulation deeper in the canyon is clearly up-canyon and weakly anticyclonic (Fig. 8a). During the third upwelling event (8 June), data at A5, 134 are also consistent with the existence of cyclonic vorticity near the rim at maximum upwelling. The doubling in thickness of the 7.0°–7.5°C layer on the upstream side of the canyon between 4 June and 6–7 June (Fig. 13) is consistent with water falling into the canyon and stretching at the initiation of upwelling, as on 21 May.

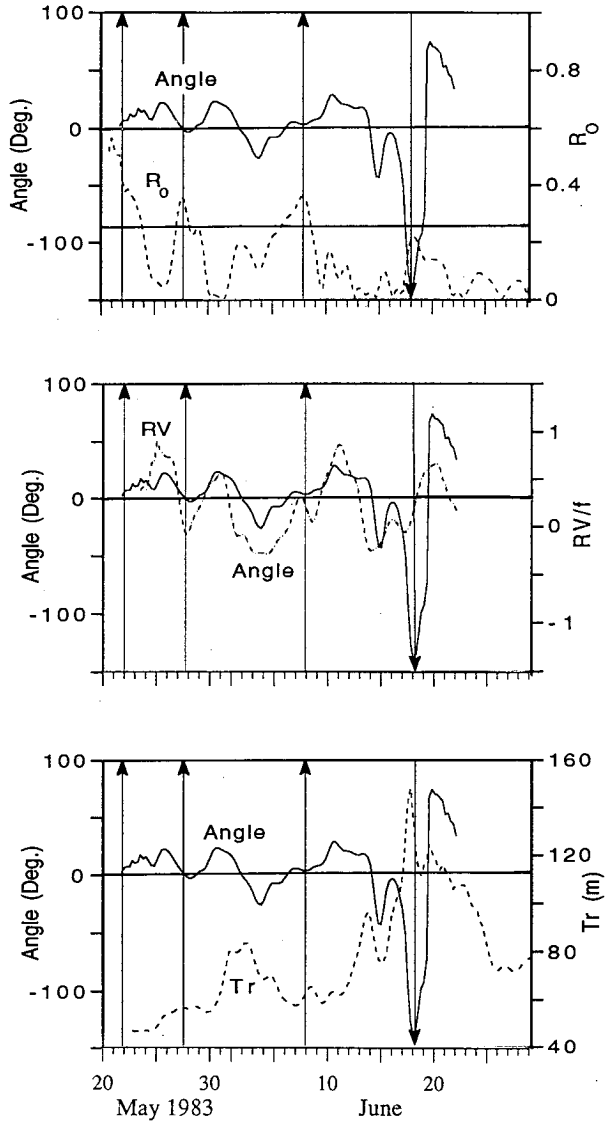

FIG. 17. Time series of the velocity direction relative to due south (the ''turning angle'') ~80 m above the canyon rim on the downstream canyon wall versus Rossby number (Ro), relative vorticity divided by *f* above the canyon (RV), and vertical trapping scale (Tr). The turning angle is positive to the east of due south (i.e., onshore).

As with vorticity estimates at midcanyon depths (near 400 m) discussed above, estimates of relative vorticity are much weaker than those of stretching vorticity. We note that estimates of stretching vorticity obtained using a monthly mean temperature profile for June as an upstream condition, rather than the ''best available'' stations two days prior to the upwelling event, are much closer to observed values of relative vorticity.

8. Models versus observations

The literature on models of submarine canyons is remarkably sparse. This may be due in part to the idea that theories developed for a hill (which are numerous by comparison) can be applied directly to a depression. This is not the case, however, because boundary layers are free to interact within a canyon; for a hill or a seamount interaction can only occur over the top or around the sides of the obstacle. The added complexity of having one open boundary, as well as the existence of strong and time variable forcing that generally occurs in coastal regions where canyons are most common, make the problem particularly difficult.

Only two models to date have addressed the dynamics of steep-sided narrow stratified submarine canyons. Allen (1996) uses three-layer models to study both spinup and steady state, linear and nonlinear dynamics of a vertical-walled canyon incising the continental slope. Klinck (1996) uses a semispectral, primitive equation, multilayer model (the ''Haidvogel'' model) to determine the steady-state response of the canyon to both upwelling- and downwelling-favorable incident flows. Allen configures one nonlinear model run specifically for the topography and stratification of Astoria Canyon. For this run, a relatively large incident velocity (~50 cm s^{-1}) was used to approximate the higher Rossby number flow observed in our field study during upwelling events. Klinck's Rossby number (~0.2) is a factor of 2 smaller than that observed in the Astoria dataset during upwelling. However, his canyon scales (aspect ratio of 0.1 and fractional height of 0.8) and one of his stratification runs ($S = 6.0$) are similar to those observed in Astoria.

To assist the reader, observational results are summarized in a series of schematics for the complete upwelling spinup and spindown cycle (Fig. 18). Although the models have not been configured for such a sequence, qualitative agreement is achieved with several aspects of the observations during spinup and at maximum upwelling.

a. Lateral velocity field

Both models show flow directed straight over the canyon at some height above the canyon rim, consistent with the observations. At deeper depths, the flow turns into the canyon. This occurs near the downstream canyon rim in the Allen model, but nearer the upstream rim in the Klinck model. The Allen results, which utilize a higher Rossby number incident flow, are more similar to the observed flow pattern. Neither model shows closed streamlines over or within the canyon, as suggested by the observations. This feature of the mean flow in the observations might be due to the wedgelike shape of the Astoria Canyon northern rim, which would tend to funnel flow across the isobaths at the apex of the funnel; alternatively, it might be due to tidal rectification.

b. Vertical velocity field

During upwelling events, the models suggest that downwelling of shelf water occurs over the upstream

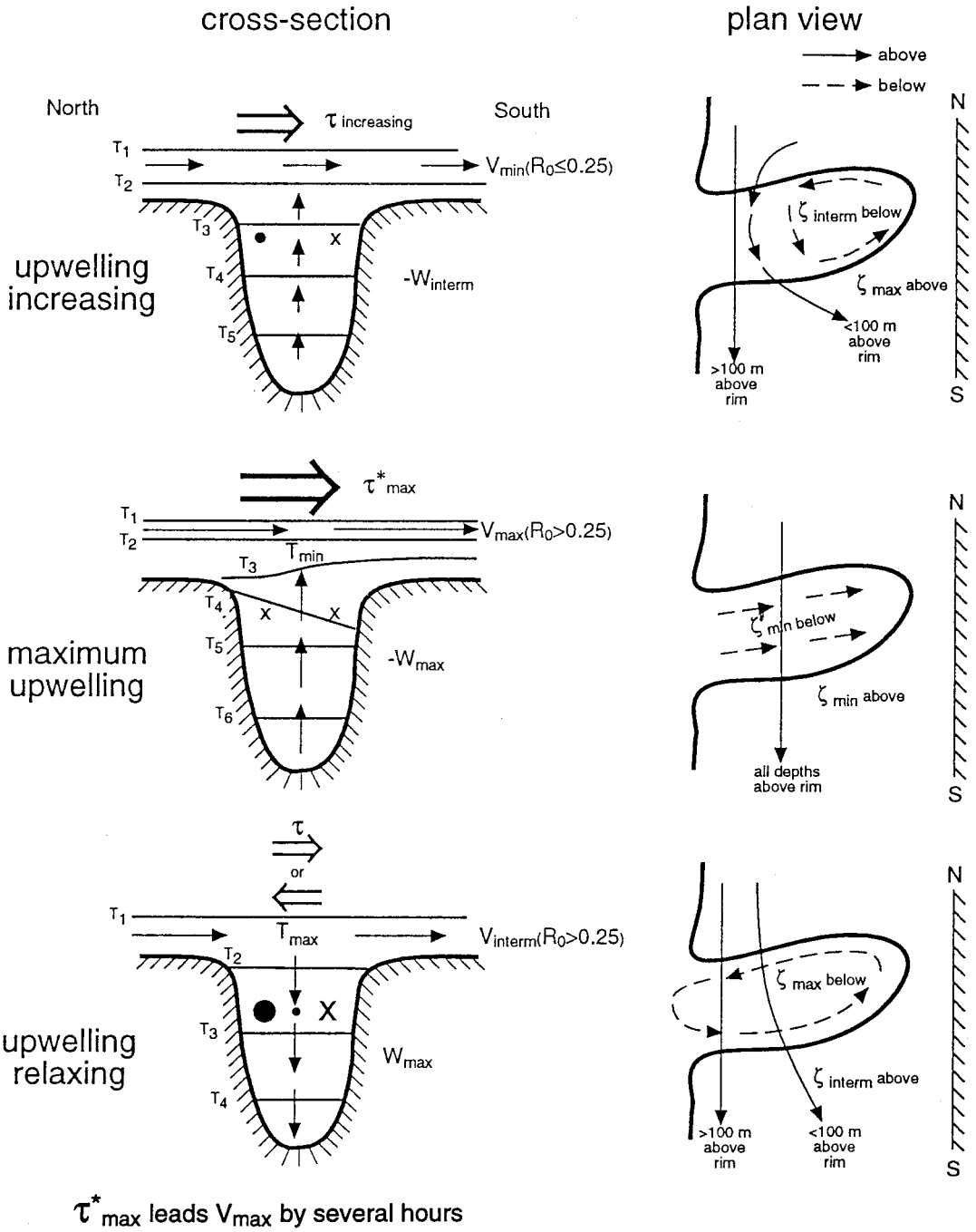

FIG. 18. Schematic illustrating data-derived characteristic timescales and spatial patterns of alongshelf wind stress (τ), velocity (V), temperature (T), and vorticity fields (ζ) at selected phases of an upwelling event.

flank of the canyon, upwelling occurs over the canyon axis and over the downstream flank, and upwelling water flows shoreward within the canyon exiting at the head and along the downstream flank. These spatial patterns are consistent with property patterns over Astoria Canyon on 21 and 22 May, 27 May, and 6–9 June (Figs. 12a,b,c and 13). Vertical velocities calculated from the data during the upwelling events are similar to those predicted by the models ($\sim$50 m d^{-1}).

Klinck's results for downwelling-favorable overflow are significantly different from those for upwelling. In particular, downwelling (on the downstream side) and upwelling (on the upstream side) are symmetric with respect to the canyon topography and no water exits the

canyon. Observed temperature contours for the one weak downwelling event discussed herein (18–19 June) are not symmetric across the canyon (Fig. 13).

c. *Vorticity field*

Allen (1996) shows cyclonic vorticity on the upstream side of the canyon near the rim and anticyclonic vorticity on the downstream side. The cyclonic vorticity near the canyon rim is associated with shelf water that has fallen into the canyon. Cyclonic vorticity is observed over about 2/3 of the canyon due to the relatively large inflow velocity and the relatively important nonlinear effects, which tend to sweep spatial patterns downstream. The spatial pattern shown in the model is very similar to that in the observations during the upwelling event of 21–22 May (Figs 12a,b). Both model and observations show deep cyclonic circulation near the head of the canyon, consistent with the CTD data, a result of layer stretching during upwelling. Modeled vorticity is generally weaker than that observed.

9. Summary

Data from a field study designed to describe the response of a narrow steep-sided submarine canyon to strong wind forcing are described. The study included an 18 element moored velocity/temperature array as well as CTD/transmissometer surveys during one strong upwelling event. For Astoria Canyon, the fractional height is 0.75, the aspect ratio is 0.2, the Rossby number ranges from 0.05 to 0.6, the stratification parameter ranges from about 16 to 8, the vertical stratification scale ranges from 40 to 80 m, and the internal Rossby radius ranges from about 60 to 30 km, for strong and weak stratification, respectively, during the period emphasized in the analysis (20 May–20 June). The data were used to provide time- and space-dependent estimates of vertical velocity and of relative and stretching vorticity. These estimates were compared with results from available models as well as with alongshelf wind and velocity incident on the canyon. The relative magnitudes and phase relationships for alongshelf wind (a proxy for wind stress), incident flow, vertical velocity, and relative vorticity during spinup and spindown from an upwelling event as deduced from the analyses are presented in Fig. 18. The most significant conclusions are summarized below.

a. *Vertical velocity*

Vertical velocity within the canyon is strongly related to (and almost in phase with) alongshelf wind stress; maximum southward wind is associated with maximum upwelling and minimum southward wind is associated with downwelling. A relationship with incident velocity is only apparent at the time of maximum upwelling when incident velocity and alongshelf wind are also approximately in phase. Upwelling occurs to depths as great as 10 m above bottom (570 m) in the canyon. The upwelling rate is spatially uniform within the canyon to zero order. The upward vertical velocity associated with upwelling reaches 50 m d^{-1}; downward vertical velocity associated with the relaxation that follows upwelling can be as great as 90 m d^{-1}.

b. *Relative vorticity*

Within the canyon, relative vorticity is strongly related to and in phase with vertical velocity (and, hence, with alongshelf wind). Cyclonic circulation is weakest during upwelling events (maxima in southward wind and upward velocity) and strongest during relaxation from upwelling (minima in southward wind or even weak northward wind and downward velocity). Above the canyon, on the other hand, relative vorticity is strongly related to and in phase with incident alongshelf flow (maximum cyclonic flow associated with minimum southward incident flow). Cyclonic circulation is observed only when the Rossby number of the incident flow drops below about 0.25.

The mean vorticity field both above and below the canyon rim has a cyclonic pattern. Below the shelf break, this pattern may be due in part to boundary separation of the slope flow; that is, flow incident on the canyon from the upstream slope may separate from the slope when the sharp turn of the canyon is encountered. Above the shelf break, where no sidewall exists, it seems more likely that the mean cyclonic pattern is due to the specific shape of the canyon topography on its upstream side. This topography tends to funnel flow west-southwest across local isobaths, causing it to stretch, and hence, acquire cyclonic vorticity. One explanation for the observed flow patterns and their temporal relationships is that a mean cyclonic circulation of unknown origin exists both above and below the canyon rim and that this mean is merely interrupted during upwelling events. Above the canyon, the cyclonic mean flow is interrupted by changes in the incident flow; namely, cyclonic vorticity is reduced during cross-canyon flow events associated with upwelling. Below the canyon rim, the mean flow is also interrupted during upwelling events, but the time scale of the interruption (i.e., the tendency for weaker cyclonic or even an anticyclonic flow pattern) is governed by the alongshelf wind stress and associated upwelling rather than by the incident flow, with its longer time scale.

With the few realizations of upwelling events available it is not possible to statistically verify whether or not the cyclonic mean flow below the canyon rim is actually caused by and/or enhanced by upwelling events. However, the fact that the strength of the cyclonic pattern observed after the three upwelling events is proportional to the magnitude of the temperature deficit produced by the upwelling event suggests that the cyclonic circulation that occurs during relaxation from

upwelling is at least consistent with being *driven* by the upwelling; that is, the canyon system does not merely relax to the same mean state after each event but is spun up to a different state of cyclonic vorticity by each event.

c. Stretching vorticity

Water properties within and above the canyon are highly active: isopleths undergo extreme vertical excursions (up to 90 m d^{-1}) as well as stretching and compression during the spinup and spindown of each wind-driven event. When upwelling is initiated, some shelf water falls into the canyon, resulting in a local increase in cyclonic vorticity on the upstream side of the canyon. Layers can also stretch as they flow over the canyon. Anticyclonic vorticity is diminished or is cyclonic in these layers relative to the anticyclonic vorticity expected in regions without canyons. Deeper within the canyon, layers are stretched due to the upwelling, leading to an increase in cyclonic relative vorticity. Maximum stretching occurs during relaxation from upwelling (i.e., during downwelling, coincident with minimum southward wind), so that the maximum cyclonic circulation within the canyon lags the maximum in southward incident velocity by 1–3 d. A reasonable statistical relationship was demonstrated between layer stretching and relative vorticity time series at locations ~40 m above and ~80 m below the canyon rim, consistent with conservation of potential vorticity.

d. Temperature

Temperature above and below the canyon rim had markedly different temporal signals, appearing to be almost out of phase. In both regions, the data support the conclusion that time changes are primarily a result of vertical, rather than lateral advection. Below the canyon rim, the time rate of change of temperature (i.e., vertical velocity) is in phase with wind; maximum cooling is associated with maximum southward wind, and maximum warming with minimum southward wind (or weak northward wind). Above the rim, on the other hand, temperature, rather than its time rate of change, is in phase with wind; coolest water is associated with maximum southward wind and warmest water with maximum relaxation from southward wind. The time rate of change of temperature *above* the canyon is in phase with vertical velocity *below* the canyon rim. These facts suggest that during upwelling the temperature above the rim reaches a minimum when southward wind is strongest. After that time, water upwelling from the canyon (where w is still negative, although somewhat reduced) exits laterally on the downstream side of the canyon rather than continuing to move upward over the canyon.

e. Model comparisons

Observations are qualitatively consistent with several aspects of model results for upwelling conditions: in particular, the asymmetric vorticity patterns near the rim during upwelling; a tendency for cyclonic vorticity at depth within the canyon during upwelling; a tendency for water to flow straight over the canyon at some height above the canyon, but to turn into the canyon at deeper depths; and the tendency for water to exit the canyon on the downstream side. The models to date offer no explanation for the existence of the mean cyclonic circulation pattern over the canyon.

One important aspect of the comparison of the observations with available models is a difference in emphasis with respect to driving mechanisms. The models, which are derived only for spinup and steady-state upwelling emphasize, and are generally driven by, alongshelf velocity. Upwelling within the canyon is driven by and enhanced relative to open slope or shelf upwelling by the cross-shelf/slope pressure gradient that balances the quasigeostrophic incident flow. This mechanism was also invoked by Freeland and Denman (1982) in a study of the Juan De Fuca Canyon. The observations presented herein emphasize the complete spinup and spindown sequence of an upwelling event. In this scenario, upwelling within the canyon appears to be much more strongly related to alongshelf wind than to incident flow. At maximum upwelling, like the models, the observations are consistent with the importance of incident flow. The difference between the models and observations arises because the spinup process is apparently not reversible: the structure of the flow during spindown is far different than during spinup, the primary difference being a bidirectional (cyclonic) rather than a unidirectional flow field. The canyon flow field during spindown appears to be unrelated to the overlying and/or incident flow and its associated pressure gradient field.

f. Discussion

Although reasonably comprehensive, the Astoria dataset was insufficient to completely resolve the important dynamics within steep-sided canyons. In particular, to determine possible dynamical contributions by lateral advection, better horizontal resolution of the temperature (density) field is required as well as additional information on upstream and downstream conditions over the shelf and slope.

Many questions regarding the interaction of strongly forced flow with steep topography such as submarine canyons remain. For example, data has been presented showing a mean cyclonic vortex over Astoria Canyon. To what extent is Astoria unique? We have speculated that the more than right angle bend in the shelf break isobaths north of the particular canyon may funnel the incident flow offshore near the apex of the bend. Northward bound flow that approaches from the south side

of the canyon might successfully follow the isobaths around the canyon (for small Ro) and yet be forced southward and offshore on its north side. This would lead to a steady cyclonic vortex under all incident conditions as observed. How do the canyon width and depth effect the response to wind forcing? To what extent is the circulation closed over the canyon; that is, to what extent would the canyon tend to trap particles? How does flow incident along the slope interact with the canyon? These and other questions are the subject of ongoing research.

Acknowledgments. The field studies described in this paper were funded by Department of Energy Contract DE-AT06-76-EV71025. Subsequent analyses were funded in part by Contract N00014-921-J-1022 from the Office of Naval Research and Grant OCE 92-17021 from the National Science Foundation. Data from June 1995 were obtained with ship support and logistics provided by Washington Sea Grant. I would like to thank the several research groups who generously provided me with important comparative data for this research. In particular, monthly mean hydrographic profiles were provided by D. Pillsbury of Oregon State University; current meter data from the SuperCODE mooring were provided by T. Strub and R. L. Smith of Oregon State University; and hydrographic data from the Washington slope and shelf on 19 May 1983 were provided by R. Reed of the NOAA Pacific Marine Environmental Laboratory. Special thanks are due to W. Fredericks who edited the data and S. Geier who performed statistical analyses. N. Kachel assisted in final data presentation. Conversations with Susan Allen at the University of British Columbia were particularly helpful to the analysis.

REFERENCES

Allen, S., 1996: Topographically generated, subinertial flows within a finite length canyon. *J. Phys. Oceanogr.,* **26,** 1608–1632.

Baines, P. G., 1983: Tidal motion in submarine canyons—A laboratory experiment. *J. Phys. Oceanogr.,* **13,** 310–328.

Bakun, A., 1975: Daily and weekly upwelling indices, west coast of North America, 1967–73. U.S. Dept. of Commerce, NOAA Tech. Rep. 16, NMFS-SSRF-693, 114 pp.

Battisti, D. S., and B. M. Hickey, 1984: Application of remote wind-forced coastal trapped wave theory to the Oregon and Washington coasts. *J. Phys. Oceanogr.,* **14,** 887–903.

Brink, K. H., D. C. Chapman, and G. R. Halliwell Jr., 1987: A stochastic model for wind-driven currents over the continental shelf. *J. Geophys. Res.,* **92** (C2), 1973–1977.

Cannon, G. A., 1972: Wind effects on currents observed in Juan de Fuca submarine canyon. *J. Phys. Oceanogr.,* **2,** 281–285.

——, R. K. Reed, and P. E. Pullen, 1985: Comparison of El Niño events off the Pacific Northwest. *El Niño North,* Washington Sea Grant, University of Washington, 75–84.

Chapman, D. C., and D. B. Haidvogel, 1992: Formation of Taylor caps over a tall isolated seamount in a stratified ocean. *Geophys. Astrophys. Fluid Dyn.,* **64,** 31–65.

Church, T. M., C. N. K. Mooers, and A. D. Voorhis, 1984: Exchange processes over a middle Atlantic bight shelfbreak canyon. *Estuar. Coastal Shelf Sci.,* **19,** 393–411.

Eide, L. I., 1979: Evidence of a topographically trapped vortex on the Norwegian continental shelf. *Deep-Sea Res.,* **26,** 601–621.

Freeland, H. J., and K. L. Denman, 1982: A topographically controlled upwelling center off southern Vancouver Island. *J. Mar. Res.,* **40**(4), 1069–1092.

Gould, W. J., R. Hendry, and H. E. Huppert, 1981: An abyssal topographic experiment. *Deep-Sea Res.,* **28A,** 409–440.

Halliwell, G. H., Jr., and J. S. Allen, 1987: Large-scale coastal wind field along the west coast of North America, 1981–1982. *J. Geophys. Res.,* **92**(C2), 1861–1884.

Hickey, B. M., 1987: The effect of a relatively narrow submarine canyon on shelf circulation. *Amer. Geophys. Union Fall Meeting,* San Francisco, CA, Eos, **68,** No. 44.

——, 1989: Patterns and processes of circulation over the Washington continental shelf and slope. *Coastal Oceanography of Washington and Oregon,* M. Landry and B. Hickey, Eds., Elsevier Science, 41–115.

——, 1995: Coastal submarine canyons. *Proc. 'Aha Huliko'a Workshop on Flow Topography Interactions,* Honolulu, HI, Office of Naval Research, 95–110.

——, E. Baker, and N. Kachel, 1986: Suspended particle movement in and around Quinault Submarine Canyon. *Mar. Geol.,* **71,** 35–83.

——, L. Pietrafesa, D. Jay, and W. C. Boicourt, 1997: The Columbia River Plume Study: Subtidal variability of the velocity and salinity fields. *J. Geophys. Res.,*

Hogg, N. A., 1973: On the stratified Taylor column. *J. Fluid Mech.,* **58,** 517–537.

Hotchkiss, F. S., and C. Wunsch, 1982: Internal waves in Hudson Canyon with possible geological implications. *Deep-Sea Res.,* **29,** 415–422.

Hunkins, K., 1988: Mean and tidal currents in Baltimore Canyon. *J. Geophys. Res.,* **93,** 6917–6929.

Huppert, H. E., and K. Bryan, 1976: Topographically generated eddies. *Deep-Sea Res.,* **23,** 655–679.

Huyer, A., and R. L. Smith, 1985: The signature of El Niño off Oregon, 1982–1983. *J. Geophys. Res.,* **90**(C4), 7133–7142.

——, B. M. Hickey, J. D. Smith, R. L. Smith, and R. D. Pillsbury, 1975: Alongshore coherence at low frequencies in currents observed over the continental shelf off Oregon and Washington. *J. Geophys. Res.,* **80,** 3495–3505.

Klinck, J. M., 1996: Circulation near submarine canyons: A modeling study. *J. Geophys. Res.,* **101**(C1), 1211–1223.

Noble, M., and B. Butman, 1989: The structure of subtidal currents within and around Lydonia Canyon: Evidence for enhanced cross-shelf fluctuations over the mouth of the canyon. *J. Geophys. Res.,* **94,** 8091–8110.

Reed, R. K., 1984: Oceanographic conditions off the Pacific Northwest following the 1982 El Niño event. *Mar. Fish. Rev.,* **46,** 7–12.

Send, U., R. C. Beardsley, and C. D. Winant, 1987: Relaxation from upwelling in the Coastal Ocean Dynamics Experiment. *J. Geophys. Res.,* **92** (C10), 1683–1698.

Shepard, F. P., N. F. Marshall, P. A. McLoughlin, and G. G. Sullivan, 1979: *Currents in Submarine Canyons and Other Seavalleys.* Amer. Assoc. Petrol. Geol., 173 pp.

Tabata, S., 1985: El Niño effects along and off the Pacific coast of Canada during 1882–1983. *El Niño North,* Washington Sea Grant, University of Washington, 85–96.

Wooster, W. S., and D. L. Fluarty, 1985: *El Niño North: Niño Effects in the Eastern Subarctic Pacific Ocean.* University of Washington, 312 pp.